Published in final edited form as:
Bioconjug Chem. 2008 October ; 19(10): 2008–2022. doi:10.1021/bc8002056.

^{64}Cu-Labeled 2-(Diphenylphosphoryl)ethyldiphenylphosphonium Cations as Highly Selective Tumor Imaging Agents:

Effects of Linkers and Chelates on Radiotracer Biodistribution Characteristics

Chang-Tong Yang[1], **Young-Seung Kim**[1], **Jianjun Wang**[1], **Lijun Wang**[1], **Jiyun Shi**[1], **Zi-Bo Li**[2], **Xiaoyuan Chen**[2], **Ming Fan**[1], **Jian-Jian Li**[1], and **Shuang Liu**[1*]

1*School of Health Sciences, Purdue University, West Lafayette, Indiana, USA*

2*Molecular Imaging Program at Stanford, Department of Radiology & Bio-X, Stanford University, Stanford, California, USA*

Abstract

Radiolabeled organic cations, such as triphenylphosphonium (TPP), represents a new class of radiotracers for imaging cancers and the transport function of multidrug resistance P-glycoproteins (particularly *MDR1* Pgp) by single photon emission computed tomography (SPECT) or positron emission tomography (PET). This report presents the synthesis and biological evaluation of ^{64}Cu-labeled 2-(diphenylphosphoryl)ethyldiphenylphosphonium (TPEP) cations as novel PET radiotracers for tumor imaging. Biodistribution studies were performed using the athymic nude mice bearing subcutaneous U87MG human glioma xenografts to explore the impact of linkers, bifunctional chelators (BFCs) and chelates on biodistribution characteristics of the ^{64}Cu-labeled TPEP cations. Metabolism studies were carried out using normal athymic nude mice to determine the metabolic stability of four ^{64}Cu radiotracers. It was found that most ^{64}Cu radiotracers described in this study have significant advantages over ^{99m}Tc-Sestamibi for their high tumor/heart and tumor/muscle ratios. Both BFCs and linkers have significant impact on biological properties of ^{64}Cu-labeled TPEP cations. For example, ^{64}Cu(DO3A-xy-TPEP) has much lower liver uptake and better tumor/liver ratios than ^{64}Cu(DO3A-xy-TPP), suggesting that TPEP is a better mitochondrion-targeting molecule than TPP. Replacing DO3A with DO2A results in ^{64}Cu(DO2A-xy-TPEP)$^{+}$, which has a lower tumor uptake than ^{64}Cu(DO3A-xy-TPEP). Substitution of DO3A with NOTA-Bn leads to a significant decrease in tumor uptake for ^{64}Cu(NOTA-Bn-xy-TPEP). The use of DOTA-Bn to replace DO3A has little impact on the tumor uptake; but the tumor/liver ratio of ^{64}Cu(DOTA-Bn-xy-TPEP)$^{-}$ is not as good as that of ^{64}Cu(DO3A-xy-TPEP), probably due to the aromatic benzene ring in DOTA-Bn. Addition of an extra acetamido group in ^{64}Cu(DOTA-xy-TPEP) results in a lower liver uptake; but tumor/liver ratios of ^{64}Cu(DOTA-xy-TPEP) and ^{64}Cu(DO3A-xy-TPEP) are well comparable due to a faster tumor washout of ^{64}Cu(DOTA-xy-TPEP). Substitution of xylene with the PEG_2 linker also leads to a significant reduction in both tumor and liver uptake. MicroPET imaging studies on ^{64}Cu (DO3A-xy-TPEP) in athymic nude mice bearing U87MG glioma xenografts showed that the tumor was clearly visualized as early as 1 h postinjection with very high T/B contrast. There was very little metabolite (<2%) detectable in the urine and feces samples for ^{64}Cu(DO3A-xy-TPEP), ^{64}Cu(DOTA-Bn-xy-TPEP)$^{-}$ and ^{64}Cu(NOTA-Bn-xy-TPEP). Considering both tumor uptake and T/B ratios (particularly tumor/heart, tumor/liver and tumor/muscle), it was concluded that ^{64}Cu(DO3A-xy-TPEP) is a promising PET radiotracer for imaging the MDR-negative tumors.

1*To whom correspondence should be addressed. School of Health Sciences, Purdue University, 550 Stadium Mall Drive, West Lafayette, IN 47907. Phone: 765-494-0236; Fax 765-496-1377; Email: lius@pharmacy.purdue.edu

Keywords

^{64}Cu-labeled TPEP cations; tumor imaging; PET radiotracers

INTRODUCTION

Alteration in the mitochondrial potential ($\Delta\psi_m$) is an important characteristic of cancer (1-4). It has been demonstrated that the mitochondrial potential in carcinoma cells is significantly higher than that in normal epithelial cells (5-9). For example, the difference in $\Delta\psi_m$ between the colon carcinoma cell line CX-1 and the control green monkey kidney epithelial cell line CV-1 was approximately 60 mV (163 mV in tumor cells versus 104 mV in normal cells). The observation that the enhanced mitochondrial potential is prevalent in tumor cell phenotype provides the conceptual basis for development of the mitochondrion-targeting pharmaceuticals and imaging probes (1-3,10-13).

Recently, we reported several ^{64}Cu-labeled triphenylphosphonium (TPP) cations as radiotracers for tumor imaging by positron emission tomography (PET) in athymic nude mice bearing U87MG human glioma xenografts (14-16). We found that that ^{64}Cu(DO3A-xy-TPP) and ^{64}Cu(DO2A-xy-TPP)$^+$ have relatively high tumor uptake with long tumor retention. The most striking difference between the ^{64}Cu-labeled TPP cations and ^{99m}Tc-Sestamibi, the most successful radiopharmaceutical currently available for both tumor and myocardial perfusion imaging, is that they all have much lower the heart uptake (<0.6% ID/g) than ^{99m}Tc-Sestamibi (~18 % ID/g) at >30 min postinjection (p.i.). Their tumor/heart ratios are >40x better than that of ^{99m}Tc-Sestamibi at 120 min p.i. The muscle uptake of ^{64}Cu(DO3A-xy-TPP) was undetectable at >30 min p.i. while ^{99m}Tc-Sestamibi has very high muscle uptake (~5 %ID/g) over the 2 h study period. Despite of their charge difference, ^{64}Cu(DO3A-xy-TPP) and ^{64}Cu (DO2A-xy-TPP)$^+$ share very similar lipophilicity, tumor uptake, tumor/heart and tumor/lung ratios. However, the positive charge in ^{64}Cu(DO2A-xy-TPP)$^+$ results in a dramatic reduction in its liver uptake. As a result, its tumor/liver ratio significantly better than that of ^{64}Cu(DO3A-xy-TPP) (16). Results from *in vitro* assays show that ^{64}Cu(DO3A-xy-TPP) is able to localize in mitochondria of glioma cells. MicroPET imaging data show that the tumor could be visualized as early as 30 min p.i. in the tumor-bearing mice administered with ^{64}Cu(DO3A-xy-TPP) (14). However, its high liver uptake remains a significant challenge for ^{64}Cu(DO3A-xy-TPP) to be clinically useful as a PET radiotracer.

To further improve the tumor uptake and tumor/background (T/B) ratios, we prepared several 2-(diphenylphosphoryl)ethyldiphenylphosphonium (TPEP) conjugates (Figure 1) and their ^{64}Cu complexes. We are particularly interested TPEP cation because the phosphoryl group (P=O) that may help improve the radiotracer hydrophilicity and excretion kinetics from the liver. Biodistribution and imaging studies were performed using athymic nude mice bearing subcutaneous U87MG glioma xenografts. The U87MG glioma cell line was chosen because it has no expression of multidrug resistance P-glycoprotein (particularly MDR1 Pgp) (17-20). This tumor-bearing animal model would allow us to evaluate the intrinsic tumor-targeting capability of ^{64}Cu radiotracers and their excretion kinetics from non-cancerous organs, such as heart, liver, lungs and muscle. The main objective of this study is to explore the impact of linkers, bifunctional chelators (BFCs) and ^{64}Cu-chelates on biodistribution characteristics and excretion kinetics of the ^{64}Cu-labeled TPEP cations.

EXPERIMENTAL

Materials and Instruments

Chemicals were purchased from *Sigma/Aldrich* (St. Louis, MO) as received. DO3A(OBu-t)$_3$ (1,4,7,10-tetraazacyclododecane-4,7,10-tris(*t*-butyl acetate)), DO2A(OBu-t)$_2$ (1,4,7,10-tetraazacyclododecane-4,7-bis(*t*-butyl acetate)), DOTA(OBu-t)$_3$-NHS (1,4,7,10-tetraazacyclododecane-1-(N-hydroxysuccinimide acetate)-4,7,10-tris(*t*-butyl acetate)) *p*-SCN-Bn-DOTA(2-(*p*-isothiocyanobenzyl)-1,4,7,10-tetraazacyclododecane-1,4,7,10-tetraacetic acid) and *p*-SCN-Bn-NOTA (2-(*p*-isothiocyanobenzyl)-1,4,7-triaazacyclononane-1,4,7-triacetic acid) were purchased from Macrocyclics Inc. (Dallas, TX). NMR (^{1}H, ^{13}C and ^{31}P) data were obtained using a Bruker DRX 300 MHz FT NMR spectrometer. Chemical shifts are reported as δ in ppm relative to TMS. ESI mass spectral data were collected using positive mode on a Finnigan LCQ classic mass spectrometer, School of Pharmacy, Purdue University. Elemental analysis was performed by Dr. H. Daniel Lee using a Perkin-Elmer Series III analyser, Department of Chemistry, Purdue University. ^{64}Cu was produced using a CS-15 biomedical cyclotron at Washington University School of Medicine by the ^{64}Ni(p,n)^{64}Cu nuclear reaction.

HPLC Methods

Method 1 used a LabAlliance semi-prep HPLC system equipped with a UV/vis detector (λ = 254 nm) and Zorbax C_{18} semi-prep column (9.4 mm × 250 mm, 100 Å pore size). The flow rate was 2.5 mL/min. The mobile phase was isocratic with 90% solvent A (0.1% acetic acid in water) and 10% solvent B (0.1% acetic acid in acetonitrile) at 0 - 5 min, followed by a gradient mobile phase going from 90% solvent A and 10% solvent B at 5 min to 60% solvent A and 40% solvent B at 20 min. Method 2 used the LabAlliance HPLC system equipped with a UV/vis detector (λ = 254 nm), a β-ram IN-US detector and Vydac C_{18} column (4.6 mm × 250 mm, 300 Å pore size). The flow rate was 1 mL/min with the mobile phase being isocratic with 90% solvent A (10 mM ammonium acetate) and 10% solvent B (acetonitrile) at 0 - 5 min, followed by a gradient mobile phase going from 10% B at 5 min to 60% B at 20 min.

(4-(Bromomethyl)benzyl)(2-(diphenylphosphoryl)ethyl)diphenylphosphonium Bromide (TPEP-xy-Br)

To a hot solution of α,α'-dibromo-*p*-xylene (528 mg, 2 mmol) in toluene (30 mL) was added slowly bis(diphenylphosphino)ethane monooxide (828 mg, 2 mmol). The mixture was heated to reflux for 20 h. The white solid was filtered, washed with toluene (20 mL) and diethyl ether (40 mL), and then dried under vacuum to give the expected intermediate product: 4-bromomethylbenzyl(diphenylphosphinoethane)phosphonium bromide (TPEP-xy-Br). The yield was 1.6 g (93 %). ^{1}H NMR ($CDCl_3$, chemical shift δ in ppm relative to TMS): 2.61(m, 2H, O=PCH_2); 3.05(m, 2H, PCH_2); 4.59 (s, 2H, CH_2Br); 4.75 (d, 2H, PCH_2, J_{PH} = 13 Hz); 6.83 (d, 4H, C_6H_4); 7.52 - 7.91 (m, 20H, C_6H_5). ESI-MS: *m/z* = 598.5 for [M^+ + H] (calcd. 598 for $C_{34}H_{32}OP_2Br^+$). TPEP-xy-Br was isolated as the bromide salt, and was used for the next step reaction without further purification.

(2-(Diphenylphosphoryl)ethyl)diphenyl(4-((4,7,10-tris(carboxymethyl)-1,4,7,10-tetraazacyclododecan-1-yl)methyl)benzyl)phosphonium Acetate (DO3A-xy-TPEP)

To a solution of TPEP-xy-Br (67.8 mg, 0.1 mmol) and DO3A(OBu-t)$_3$ (51.5 mg, 0.1 mmol) in dry DMF (3 mL) was added triethylamine (0.07 mL, 0.5 mmol). The reaction mixture was stirred at 50 °C overnight. After complete removal of volatiles, the residue was dissolved in 12 N HCl (2 mL). The resulting solution was stirred at room temperature for 30 min. Volatiles were completely removed under vacuum. The residue was then dissolved in water (3 mL), was then subjected to HPLC purification (Method 1). The fractions at ~17.3 min were collected,

combined, and lyophilized to give a white powder. The yield was 30.1 mg (33 %). ^{1}H NMR (D_2O, chemical shift δ in ppm relative to TMS): 1.89 (s, 3H, CH_3COO^-); 2.80 - 3.7 (m, 26H); 3.67 (s, 2H); 4.29 (d, 2H, PC*H*$_2$, J_{PH} = 13 Hz); 6.71(d, 2H, C_6H_4); 7.18 (d, 2H, C_6H_4); 7.38 - 7.67 (m, 20H, C_6H_5). ESI-MS: *m/z* = 863.2 for $[M + H]^+$ (calcd. 863 for $[C_{48}H_{57}N_4O_7P_2]^+$). Anal. Calcd. for $C_{48}H_{57}N_4O_7P_2 \cdot CH_3CO_2 \cdot 5H_2O$: C, 59.28; H, 6.96; N, 5.53. Found: C, 59.48; H, 6.85; N, 5.71.

(4-((4,10-Bis(carboxymethyl)-1,4,7,10-tetraazacyclododecan-1-yl)methyl)benzyl)(2-(diphenylphosphoryl)ethyl)diphenylphosphonium Acetate (DO2A-xy-TPEP)

To a solution of TPEP-xy-Br (67.8 mg, 0.1 mmol) and DO2A(OBu-t)$_2$ (80 mg, 0.2 mmol) in dry DMF (3 mL) was added triethylamine (0.07 mL, 0.5 mmol). The mixture was stirred at room temperature overnight. After complete removal of volatiles, the residue was dissolved in 12 N HCl (3 mL). The solution was stirred at room temperature for 30 min. Volatiles were removed completely on a rotary evaporator. The residue was then dissolved in water (3 mL), and the product was separated from the mixture by HPLC purification (Method 1). The fractions at ~11.8 min were collected, combined and lyophilized to give a white powder. The yield was 28.5 mg (33 %). ^{1}H NMR (in $CDCl_3$): 1.89 (s, 3H, CH_3COO^-); 2.42 (m, 4H); 2.70 - 3.01 (m, 20H); 3.40 (s, NC*H*$_2$); 4.85 (d, 2H, PC*H*$_2$, J_{PH} = 13 Hz); 6.78 (d, 2H, C_6H_4); 7.30 (d, 2H, C_6H_4); 7.47 - 7.83 (m, 20H, C_6H_5). ESI-MS: *m/z* = 805.4 for $[M + H]^+$ (805 calcd. for $C_{46}H_{55}N_4O_5P_2^+$). Anal. Calcd. for $C_{46}H_{55}N_4O_5P_2 \cdot CH_3CO_2 \cdot 6.5H_2O$: C, 58.71; H, 7.29; N, 5.71. Found: C, 58.50; H, 6.89; N, 5.77.

(2-(Diphenylphosphoryl)ethyl)diphenyl(2-(2-(2-(tosyloxy)ethoxy)ethoxy)ethyl) phosphonium Tosylate (TPEP-PEG$_2$-OTs)

TsO-PEG2-OTs was prepared using the literature procedure.[16] TPEP mono-oxide (104 mg, 0.25 mmol) and TsO-PEG$_2$-OTs (230 mg, 0.5 mmol) were suspended in dry toluene (10 mL). The mixture was heated to reflux for 20 h. Volatiles were removed under vacuum. The residue was dissolved in 50% DMF/H_2O mixture. The resulting solution was subject to HPLC purification (Method 1). The fractions at ~16.5 min were collected and lyophilized to give a white solid. The yield was 65.5 mg (30%). ^{1}H NMR (in $CDCl_3$): 2.33 (s, 3 H, *CH*$_3$), 2.43 (s, 3 H, *CH*$_3$), 2.75 (m, 2H, O=P*CH*$_2$), 3.17-3.71 (m, 12 H), 4.09 (t, 2H, P*CH*$_2$), 7.12 (d, 2 H, *J* = 7.8 Hz), 7.32-7.78 (m, 26 H). ESI-MS: *m/z* = 701.17 for $[M]^+$ (calcd. 701 for $[C_{39}H_{43}O_6P_2S]^+$).

(2-(Diphenylphosphoryl)ethyl)diphenyl(2-(2-(2-(4,7,10-tris(carboxymethyl)-1,4,7,10-tetraazacyclododecan-1-yl)ethoxy)ethoxy)ethyl)phosphonium Tosylate (DO3A-PEG2-TPEP)

TPEP-PEG$_2$-OTs (24 mg, 0.027 mmol) and DO3A(t-Bu)$_3$ (14 mg, 0.027 mmol) were dissolved in dry DMF (3 mL). After addition of Et_3N (30 μL, 0.20 mmol), the solution was stirred at room temperature for 20 h. After removal of volatiles, the residue was dissolved in 12 N HCl (3 mL). The solution was stirred for 2 h. After complete removal of volatiles under vacuum, the residue was dissolved in water (3 mL). The resulting solution was subjected to HPLC purification (Method 1). The fractions at ~10 min were collected, combined and lyophilized to give a white powder. The yield was 8.5 mg (30%). ^{1}H NMR (in $CDCl_3$): 2.21 (s, 3H, *CH*$_3$), 2.39-3.63 (m, 38 H), 7.19 (d, 2H), 7.35-7.72 (m, 22 H). ^{31}P NMR: 32.41 (d, *J* = 54.4 Hz), 42.84 (d, *J* = 54.4 Hz). ESI-MS: *m/z* = 875.01 for $[M]^+$ (calcd. 875 for $[C_{46}H_{61}N_4O_9P_2]^+$). Anal. Calcd. for $C_{46}H_{61}N_4O_9P_2 \cdot CH_3C_6H_4SO_3 \cdot H_2O$: C, 59.76; H, 6.62; N, 5.71. Found: C, 59.48; H, 6.85; N, 5.62.

(4-((1,3-Dioxoisoindolin-2-yl)methyl)benzyl)(2-(diphenylphosphoryl)ethyl)diphenylphosphonium Bromide (TPEP-xy-PA)

TPEP-xy-Br (340 mg, 0.5 mmol) and potassium pthalimide (110 mg, 0.6 mmol) were suspended in acetonitrile (10 mL). The suspension was heated to reflux for 24 h. The solid was filtered and the filtrate was dried under vacuum to give a light-yellow solid (300 mg, 0.40 mmol, 80%). ^{1}H NMR (in $CDCl_3$): 2.83 (m, 2 H), 3.14 (m, 2 H), 4.66 (s, 2 H, CH_2N), 5.14 (d, 2 H, PCH_2, J_{PH} = 14.4 Hz), 6.80 (dd, 2 H, J = 8.1, 2.7 Hz), 6.93 (d, 2 H, J = 8.1 Hz), 7.45-7.90 (m, 20 H), 8.05-8.18 (m, 4 H). ^{31}P NMR: 28.9 (d, J = 53.1 Hz), 33.0 (d, J = 53.1 Hz). ESI-MS: m/z = 664.03 for $[M]^+$ (calcd. 664 for $[C_{42}H_{36}NO_3P_2]^+$).

(4-(Aminomethyl)benzyl)(2-(diphenylphosphoryl)ethyl)diphenylphosphonium (TPEP-xy-NH_2)

The TPEP-xy-PA intermediate (300 mg, 0.40 mmol) and 0.53 mL of aqueous hydrazine (55%, 88 mmol) were added into absolute ethanol (20 mL). The resulting solution was heated to reflux for 20 h. Volatiles were removed under vacuum. The light-yellow solid was dissolved in dichloromethane (20 mL). After filtration, the solvent was evaporated to get light-yellow solid. The yield was 230 mg (92%). ^{1}H NMR (in $CDCl_3$): 2.88 (m, 2 H), 3.10 (m, 2 H), 3.72 (s, 2 H, CH_2N), 5.14 (d, 2 H, PCH_2, J_{PH} = 14.4 Hz), 6.85 (m, 4 H), 7.42-7.85 (m, 16 H), 8.05-8.15 (m, 4 H). ^{31}P NMR: 28.8 (d, J = 51.7 Hz), 33.1 (d, J = 51.7 Hz). ESI-MS: m/z = 534.11 for $[M]^+$ (calcd. 534 for $[C_{34}H_{34}NOP_2]^+$).

(2-(Diphenylphosphoryl)ethyl)diphenyl(4-((2-(4,7,10-tris(carboxymethyl)-1,4,7,10-tetraazacyclododecan-1-yl)acetamido)methyl)benzyl)phosphonium Acetate (DOTA-xy-TPEP)

TPEP-xy-NH_2 (10 mg, 0.01 mmol) and PF_6 salt of DOTA(t-Bu)$_3$-NHS (6.7 mg, 0.01 mmol) were dissolved in dry DMF (3 mL). Upon addition of triethylamine (44 μL, 0.32 mmol), the resulting mixture was stirred at room temperature for 20 h. After removal of volatiles, the residue was dissolved in the concentrated HCl (3 mL). The solution was then stirred at room temperature for 2 h. Volatiles were completely removed under vacuum, and the residue was dissolved in water (3 mL). The product was separated from the mixture by HPLC (Method 1). The fractions at ~18 min were collected and lyophilized to give a white powder. The yield was 5.6 mg (56%). ^{1}H NMR (in D_2O): 1.88 (s, 3H, CH_3COO^-); 2.55-3.35 (m, 26 H), 3.59 (d, 2 H, NCH_2), 4.12 (s, 2 H, CH_2NH), 4.21 (d, 2 H, PCH_2, J = 14.7 Hz), 6.60 (dd, 2 H, J = 7.8 and 2.2 Hz), 6.94 (d, 2 H, J = 7.8), 7.32-7.75 (m, 20 H). ^{31}P NMR: 30.64 (d, J = 53.0 Hz), 43.09 (d, J = 53.0 Hz). ESI-MS: m/z = 920.1 for $[M]^+$ (calcd. 920 for $[C_{50}H_{60}N_5O_8P_2]^+$). Anal. Calcd. for $C_{50}H_{60}N_5O_8P_2 \cdot CH_3CO_2 \cdot 2H_2O$: C, 61.47; H, 6.65; N, 6.89. Found: C, 61.11; H, 6.53; N, 6.96.

(2-(Diphenylphosphoryl)ethyl)diphenyl(4-((3-(4-((1,4,7,10-tetrakis(carboxymethyl)-1,4,7,10-tetraazacyclododecan-2-yl)methyl)phenyl)thioureido)methyl)benzyl)phosphonium Acetate (DOTA-Bn-xy-TPEP)

TPEP-xy-NH_2 (6 mg, 0.01 mmol) and p-SCN-Bn-DOTA (6.7 mg, 0.01 mmol) were dissolved in the equal volume mixture (2 mL) of DMF and water. The pH value in the mixture was adjusted to 8.5 with 1 N NaOH. The resulting mixture was stirred at room temperature overnight and then purified by HPLC (Method 1). The fractions at ~17.8 min were collected. Lyophilization of the collected fractions gave a white powder. The yield was 6.3 mg (56%). ^{1}H NMR (in D_2O): 1.90 (s, 3H, CH_3COO^-); 2.35-3.82 (m, 29 H), 4.22 (d, 2 H, PCH_2, J_{PH} = 16.2 Hz), 4.49 (s, 2 H, CH_2NH), 6.55 (dd, 2 H), 6.78 (m, 2 H), 7.16 (m, 2 H), 7.32-7.53 (m, 20 H), 7.69 (m, 3 H). ^{31}P NMR: 30.62 (d, J = 52.4 Hz) and 42.84 (d, J = 52.4 Hz). ESI-MS: m/z = 1085.22 for $[M]^+$ (calcd. 1085 for $[C_{58}H_{67}N_6O_9P_2S]^+$). Anal. Calcd. for $C_{58}H_{67}N_6O_9P_2S \cdot CH_3CO_2$: C, 62.92; H, 6.16; N, 7.34. Found: C, 62.80; H, 6.46; N, 7.39.

(2-(Diphenylphosphoryl)ethyl)diphenyl(4-((3-(4-((1,4,7-tris(carboxymethyl)-1,4,7-triazonan-2-yl)methyl)phenyl)thioureido)methyl)benzyl)phosphonium Acetate (NOTA-Bn-xy-TPEP)

NOTA-Bn-xy-TPEP was prepared according to the same procedure for DOTA-Bn-xy-TPEP using TPEP-xy-NH_2 (5 mg, 0.008 mmol) and p-SCN-Bn-NOTA (3.7 mg, 0.008 mmol). The fractions at ~15.1 min (Method 1) were collected, combined and lyophilized to give a white powder. The yield was 4.6 mg (54%). ^{1}H NMR (in D_2O): 1.92 (s, 3H, CH_3COO^-); 2.35-3.70 (m, 23 H), 4.47 (s, 2 H, C*H*$_2$NH), 4.21 (d, 2 H, PC*H*$_2$, J_{PH} = 14.1 Hz), 6.53 (d, 2 H), 6.86 (d, 2 H), 7.02-7.22 (m, 4 H), 7.30-7.56 (m, 18 H), 7.68(m, 2 H). ^{31}P NMR: 30.38 (d, *J* = 52.6 Hz), 42.66 (d, *J* = 52.6 Hz). ESI-MS: *m/z* = 984.06 for $[M]^+$ (calcd 984 for $[C_{54}H_{60}N_5O_7P_2S]^+$). Anal. Calcd. for $C_{54}H_{60}N_5O_7P_2S{\cdot}CH_3CO_2$: C, 64.42; H, 6.08; N, 6.71. Found: C, 64.29; H, 6.00; N, 6.83.

^{64}Cu-Labeling

To a 5 mL vial were added 0.5 mL 0.1 M NaOAc buffer (pH = 6.9) containing 50 μg of the TPEP conjugate and 0.12 mL of $^{64}CuCl_2$ solution (1.0 - 2.0 mCi) in 0.05 N HCl. The final pH was 5.0 - 5.5. The mixture was heated at 100 °C for 30 min. After cooling to room temperature, a sample of resulting solution was analyzed by radio-HPLC (Method 2). The radiochemical purity (RCP) was >90% for all ^{64}Cu radiotracers with specific activity being ~50 Ci/mmol. RCP data and HPLC retention times of ^{64}Cu radiotracers are listed in Table 1.

Dose Preparation

All newly synthesized ^{64}Cu radiotracers were purified by HPLC before being used for biodistribution studies. Volatiles in the HPLC mobile phases were completely removed under vacuum (< 10 mmHg) at 40 - 50 °C. The residue was dissolved in saline to ~25 μCi/mL. The resulting solution was filtered with a 0.20 μ syringe-driven filter unit to eliminate any particles. Each animal was administered intravenously with ~0.10 mL of the dose solution. For the imaging study, ^{64}Cu(DO3A-xy-TPEP) was prepared and the resulting mixture was used without purification. The reaction mixture was diluted to ~5 mCi/mL with saline. The injected dose for each tumor-bearing mouse was about 250 μCi of ^{64}Cu(DO3A-xy-TPEP).

Solution Stability

For solution stability, ^{64}Cu(DO3A-xy-TPEP), ^{64}Cu(DO2A-xy-TPEP), ^{64}Cu(NOTA-Bn-xy-TPEP) and ^{64}Cu(DOTA-Bn-xy-TPEP)$^-$ were prepared and purified by HPLC (Method 2). Volatiles in the HPLC mobile phase were removed under vacuum. The residue was dissolved in saline to ~1 mCi/mL. Samples were analyzed by HPLC (Method 2) at 0, 1, 2, 4 and 12 h post purification. In the EDTA challenge experiment, the HPLC purified ^{64}Cu radiotracers were dissolved in 25 mM phosphate buffer (pH = 7.4) containing EDTA (1 mg/mL) to 1 mCi/mL. Samples of the resulting solution were analyzed by radio-HPLC (Method 2) at 0, 1, 2, 4 and 12 h post purification.

Partition Coefficient

All new ^{64}Cu radiotracers were purified before being used for partition coefficient determination. HPLC purification is needed to eliminate potential interference from other radio-impurities. After complete removal of volatiles in the HPLC mobile phases under vacuum (< 10 mmHg) at 40 - 50 °C, the residue was dissolved in a mixture of 3 mL saline and 3 mL n-octanol. The mixture was stirred vigorously for 20 min at room temperature, and was then transferred to an Eppendorf microcentrifuge tube. The tube was centrifuged at 12,500 rpm for 5 min. Samples in triplets from n-octanol and aqueous layers were obtained, and were counted a Perkin Elmer Wizard - 1480 automatic γ-counter (Shelton, CT). The log P value was reported as an average of the data obtained in three independent measurements.

Tumor-Bearing Animal Model

The ex-vivo biodistribution studies were performed using athymic nude mice bearing U87MG human glioma xenografts in compliance the NIH animal experiment guidelines (*Principles of Laboratory Animal Care*, NIH Publication No. 86-23, revised 1985). The animal protocol has been approved by Purdue University Animal Care and Use Committee (PACUC). Female athymic nu/nu mice (4 - 5 weeks of age) were purchased from Harlan (Charles River, MA). Each mouse was implanted with 5×10^6 the U87MG glioma cells into the upper shoulder flank. Three to four weeks after inoculation, the tumor size was in the range of 0.3 - 0.6 g, and animals were used for both biodistribution and imaging studies.

Biodistribution Protocol

Twelve tumor-bearing mice (20 - 25 g) were randomly divided into four groups. The ^{64}Cu radiotracer (~2.5 μCi dissolved in 0.1 mL saline) was administered each animal via tail vein. Three animals were sacrificed by sodium pentobarbital overdose (100 mg/kg) at 5, 30, 60, and 120 min p.i. The blood sample was withdrawn from the heart. Organs were excised, washed with saline, dried with absorbent tissue, weighed, and counted on a Perkin Elmer Wizard - 1480 γ-counter (Shelton, CT). Organs of interest included tumor, brain, heart, spleen, lungs, liver, kidneys, muscle and intestine. The organ uptake was calculated as a percentage of the injected dose per organ (%ID/organ) and a percentage of the injected dose per gram of organ tissue (%ID/g).

Calibration of microPET

Scanner activity calibration was performed to map between microPET image units and units of activity concentration. A pre-weighed 50 mL centrifuge tube was filled with solution containing $^{64}CuCl_2$ (~ 9.3 MBq as determined by the dose calibrator) was used to simulate whole body of the mouse. This tube was weighed, centered in the scanner aperture, and imaged for 30 min static image. From the sample weight and the density of 1 g/mL, the activity concentration was calculated as μCi/mL. Eight planes were acquired in the coronal section. A rectangular region of interest (ROI) (counts/pixel/s) was drawn on the middle of 8 coronal planes. The calibration factor was obtained by dividing the known radioactivity in the cylinder (μCi/mL) by the image ROI. This calibration factor was determined periodically and did not vary significantly with time.

MicroPET Imaging

MicroPET imaging of the tumor-bearing mice was performed using a microPET R4 rodent model scanner (Concorde Microsystems, Knoxville, TN). The tumor-bearing mice (n = 3) were imaged in the prone position in the microPET scanner. Each tumor-bearing mouse was injected with ~250 μCi of ^{64}Cu(DO3A-xy-TPEP) via the tail vein, then anesthetized with 2% isoflurane and placed near the center of the FOV where the highest resolution and sensitivity are obtained. Multiple static scans were obtained at 0.5, 1.0, 2 and 20 h p.i. The images were reconstructed by a two-dimensional ordered subsets expectation maximum (OSEM) algorithm. No correction was necessary for attenuation or scatter. At each microPET scan, the ROIs were drawn over the tumor and major organs on decay-corrected whole-body coronal images. The average radioactivity concentration within the tumor or an organ was obtained from mean pixel values within the multiple ROI volume, which were converted to counts/mL/min by using the calibration constant C. Assuming that the tissue density is 1 g/mL, the ROIs were converted to counts/g/min, and were then divided by the total administered activity to obtain an imaging ROI-derived percentage administered activity per gram of tissue (%ID/g).

Metabolism

Metabolic stability was evaluated in normal nude mice for ^{64}Cu(DO3A-xy-TPEP), ^{64}Cu(DOTA-xy-TPEP), ^{64}Cu(DOTA-Bn-xy-TPEP)$^{-}$ and ^{64}Cu(NOTA-Bn-xy-TPEP). Each mouse was administered with 100 μCi of ^{64}Cu radiotracer via tail vein. Urine samples were collected at 30 and 120 min p.i. by manual void, and were mixed with equal volume of acetonitrile. The mixture was centrifuged at 8,000 rpm. The supernatant was collected and filtered through a 0.20 μm Millex-LG syringe-driven filter unit to remove the precipitate and large proteins. The filtrate was analyzed by radio-HPLC (Method 2). The feces samples were collected at ~120 min p.i., and were suspended in a mixture of 50% acetonitrile aqueous solution. The mixture was vortexed for 5 - 10 min. After centrifuging at 8,000 rpm for 5 min, the supernatant was collected and passed through a 0.20 μm Millex-LG syringe-driven filter unit to remove the precipitate or particles. The filtrate was then analyzed by radio-HPLC (Method 2).

Stability of ^{64}Cu(DO3A-xy-TPEP) in Liver

The liver tissue was harvested at 120 min p.i. from the mouse administered with ^{64}Cu(DO3A-xy-TPEP) (~100 μCi), counted in a γ-counter (Perkin Elmer Wizard - 1480, Shelton, CT) for total liver radioactivity, and was then homogenized. The homogenate was mixed with 2 mL of saline. After centrifuging at 8,000 rpm for 5 min, the supernatant was collected and counted on a γ-counter (Perkin Elmer Wizard - 1480, Shelton, CT) to determine the percentage of radioactivity recovery. After filtration through a 0.20 μm Millex-LG filter unit to remove foreign particles, the filtrate was then analyzed by radio-HPLC (Method 2).

Data and Statistical Analysis

The biodistribution data and T/B ratios are reported as an average plus the standard variation based on results from three tumor-bearing mice at each time point. Comparison between two different radiotracers was made using the two-way ANOVA test (GraphPad Prim 5.0, San Diego, CA). The level of significance was set at $p < 0.05$.

RESULTS

Synthesis of TPEP Conjugates

DO3A-xy-TPEP, DO2A-xy-TPEP and DO3A-PEG$_2$-TPEP were prepared according to Chart I. They were designed to examine the impact of linkers (xy vs. PEG$_2$) and molecular charge (^{64}Cu-DO3A vs. ^{64}Cu-DO2A) on organ uptake and excretion kinetics of the ^{64}Cu radiotracers. DOTA-xy-TPEP, DOTA-Bn-xy-TPEP, NOTA-Bn-xy-TPEP were designed to examine the impact of BFCs (DO3A vs. DOTA, DOTA-Bn and NOTA-Bn) on biodistribution patterns of ^{64}Culabeled TPEP cations. DOTA-xy-TPEP was prepared from the reaction of DOTA(OBu-t)$_3$-NHS with TPEP-xy-NH$_2$ (Chart II), followed by hydrolysis of DOTA(OBu-t)$_3$-xy-TPEP in 12 N HCl. DOTA-Bn-xy-TPEP and NOTA-Bn-xy-TPEP were prepared by reacting TPEP-xy-NH$_2$ with *p*-SCN-Bn-DOTA and *p*-SCN-Bn-NOTA (Chart II), respectively. All the TPEP conjugates, except DO3A-PEG$_2$-TPEP, were obtained as acetate salts after lyophilization since the HPLC mobile phases contain 0.1% acetic acid. They all have been characterized by NMR, ESI-MS and elemental analysis. The purity of the TPEP conjugates were >95% before being used for ^{64}Cu-labeling. Both TPEP-PEG$_2$ and DO3A-PEG$_2$-TPEP were isolated as tosylate salts, as evidenced by the proton signals of tosylate anion in their ^{1}H NMR spectra, and the molecular ion at *m/z* = 171 in their negative mode ESI-mass spectra. It is not clear why TPEP-PEG$_2$ and DO3A-PEG$_2$-TPEP were obtained as tosylate salts while other TPEP conjugates were isolated as acetate salts after HPLC purification and lyophilization.

Radiochemistry

All ^{64}Cu radiotracers were prepared by reacting $^{64}CuCl_2$ with the TPEP conjugate in 0.1 M NaOAc buffer (pH = 5.0 - 5.5) at 100 °C for 30 min, and were analyzed using the same reversed-phase HPLC method (Method 2). The RCP for all new ^{64}Cu radiotracers was >95% with the specific activity being >50 Ci/mmol. Their partition coefficients were determined in a 50%: 50% (v:v) mixture of n-octanol and 25 mM phosphate buffer (pH = 7.4). Their log P values and HPLC retention times are listed in Table 1. All new ^{64}Cu radiotracers are very hydrophilic with their log P values < -1.50. BFCs and linkers have a significant impact on lipophilicity of the ^{64}Cu radiotracer. For example, ^{64}Cu(DOTA-xy-TPEP) (log P = -2.45 ± 0.02) is more hydrophilic than ^{64}Cu(DO3A-xy-TPEP) (log P = -1.69 ± 0.11) due to the replacement of DO3A with DOTA. Substitution of xylene with the PEG_2 linker made ^{64}Cu(DO3A-PEG_2-TPEP) (log P = -3.06 ± 0.08) more hydrophilic than ^{64}Cu(DO3A-xy-TPEP). Despite their charge difference, the lipophilicity of ^{64}Cu(DO3A-xy-TPEP) (log P = -1.69 ± 0.11) was close to that of $^{64}Cu(DO2A\text{-}xy\text{-}TPEP)^+$ (log P = -1.90 ± 0.10). ^{64}Cu(NOTA-Bn-xy-TPEP) (log P = -1.75 ± 0.03) also shared the similar lipophilicity with ^{64}Cu(DO3A-xy-TPEP) in spite of the extra aromatic phenyl group. Since NOTA-Bn has the same number of acetate chelating arms as DO3A, ^{64}Cu in ^{64}Cu-NOTA-Bn is most likely coordinated by six N_3O_3 donor atoms in the distorted-pseudo-prismatic coordination geometry as observed in the solid state structure of $Na[Cu(NOTA)]\cdot 2NaBr\cdot 8H_2O$ (21). Therefore, it is reasonable to believe that ^{64}Cu(NOTA-Bn-xy-TPEP) exists as its Zwitterion form. In $^{64}Cu(DOTA\text{-}Bn\text{-}xy\text{-}TPEP)^-$, however, ^{64}Cu is likely coordinated by only six (N_4O_2) of its eight donor atoms (N_4O_4) in the distorted octahedral coordination geometry, as observed in the solid state structure of $Cu(DOTA)^{2-}$ with two acetate-O atoms remaining uncoordinated (22,23). The extra acetate groups will results in the negative molecular charge under physiological conditions (pH = 7.4), $^{64}Cu(DOTA\text{-}Bn\text{-}xy\text{-}TPEP)^-$ (log P = -1.92 ± 0.03) is slightly more hydrophilic than ^{64}Cu(DO3A-xy-TPEP).

Solution Stability

The EDTA challenge experiment was used to study the solution stability of ^{64}Cu(DO3A-xy-TPEP), $^{64}Cu(DO2A\text{-}xy\text{-}TPEP)^+$, $^{64}Cu(DOTA\text{-}Bn\text{-}xy\text{-}TPEP)^-$ and ^{64}Cu(NOTA-Bn-xy-TPEP). These four ^{64}Cu radiotracers were selected because they represent four different types of BFCs (DO3A, DO2A, DOTA-Bn and NOTA-Bn) for ^{64}Cu chelation. The purpose of these studies was to demonstrate that the ^{64}Cu radiotracer remains intact before being injected into the tumor-bearing mice. Table 2 summarizes their solution stability data in the presence of excess EDTA (3 mM, pH = 7.4). On the basis of these data, it becomes quite clear that all four ^{64}Cu-labeled TPEP cations are stable for >12 h in the presence of 3 mM EDTA (25 mM phosphate buffer, pH = 7.4).

Biodistribution Data

Biodistribution characteristics of six new ^{64}Cu radiotracers were evaluated in athymic nude mice bearing U87MG glioma xenografts. The Western Blot data (Figure SI) clearly demonstrated that there is no MDR1 Pgp expression on U87MG glioma xenografts. Selected biodistribution data and T/B ratios are listed in Tables 3 and 4, respectively. Detailed biodistribution data and T/B ratios are summarized in Tables SI-SVI. The main objective of these studies was to explore the impact of linkers and ^{64}Cu chelates on biodistribution characteristics and excretion kinetics of ^{64}Cu-labeled TPEP cations.

Comparison with $_{99m}$Tc-Sestamibi and $_{64}$Cu(DO3A-xy-TPP)

Figure 2 compares the selected organ uptake and T/B ratios between ^{64}Cu(DO3A-xy-TPEP), ^{64}Cu(DO3A-xy-TPP) and ^{99m}Tc-Sestamibi. This comparison allows us to demonstrate advantages of the ^{64}Cu-labeled TPEP cations over ^{99m}Tc-Sestamibi with respect to tumor uptake and T/B ratios, and to assess the impact of “targeting moiety” (TPEP vs. TPP) on

biodistribution patterns of ^{64}Cu radiotracer. ^{99m}Tc-Sestamibi was used as the "control" since it has been clinically used for imaging tumors and monitoring the tumor MDR transport functions (25-33). Biodistribution data and T/B ratios for ^{64}Cu(DO3A-xy-TPP) and ^{99m}Tc-Sestamibi were obtained from our previous report (14).

The most striking differences between ^{64}Cu(DO3A-xy-TPEP) and ^{99m}Tc-Sestamibi are their uptake in the heart and muscle and their T/B (tumor/heart, tumor/liver, tumor/lung and tumor/muscle) ratios. For example, the heart uptake of ^{64}Cu(DO3A-xy-TPEP) was <1% ID/g at >30 min p.i., while the heart uptake of ^{99m}Tc-Sestamibi was 19.22 ± 7.62 at 5 min p.i. and 19.19 ± 5.32 %ID/g at 120 min p.i. (14). The muscle uptake of ^{64}Cu(DO3A-xy-TPEP) was almost undetectable at ≥60 min p.i. while ^{99m}Tc-Sestamibi had a high muscle uptake (4.84 ± 1.22 and 5.45 ± 1.24 %ID/g at 5 and 120 min p.i., respectively) over the 2 h period (Table 3). ^{64}Cu(DO3A-xy-TPEP) had the tumor uptake that is significantly (p <0.05) higher than that of ^{99m}Tc-Sestamibi at all four time points. The tumor/heart ratio of ^{64}Cu(DO3A-xy-TPEP) at 120 min p.i. was more than 50x better than that of ^{99m}Tc-Sestamibi. Its tumor/lung and tumor/liver ratios were much better than those of ^{99m}Tc-Sestamibi (Figure 3). ^{64}Cu(DO3A-xy-TPEP) had a tumor uptake that is well comparable to that of ^{64}Cu(DO3A-xy-TPP) at >30 min p.i.; but its liver uptake was significantly lower (p < 0.01) than that of ^{64}Cu(DO3A-xy-TPP) at all four time points (Table 3). As a result, ^{64}Cu(DO3A-xy-TPEP) has tumor/liver ratios >3x better than those of ^{64}Cu(DO3A-xy-TPP). Thus, TPEP is better than TPP as the mitochondrion-targeting molecules.

Impact of BFCs

Figure 3 compares the organ uptake (heart, liver and muscle) and T/B ratios of ^{64}Cu(DO3A-xy-TPEP), ^{64}Cu(DO2A-xy-TPEP)$^{+}$, ^{64}Cu(DOTA-Bn-xy-TPEP)$^{-}$ and ^{64}Cu(NOTA-Bn-xy-TPEP). This comparison allows us to assess the impact of BFCs on biological properties of ^{64}Cu radiotracers. ^{64}Cu(DO3A-xy-TPEP) has the lipophilicity (log P = -1.69 ± 0.11) close to that of ^{64}Cu(DO2A-xy-TPEP)$^{+}$ (log p = -1.90 ± 0.10) despite their different charge. While the tumor uptake of ^{64}Cu(DO3A-xy-TPEP) remained unchanged between 30 and 120 min p.i., there was a significant tumor washout for ^{64}Cu(DO2A-xy-TPEP)$^{+}$ over the 2 h period. The liver uptake of ^{64}Cu(DO2A-xy-TPEP)$^{+}$ was significantly (p < 0.01) lower than that of ^{64}Cu(DO3A-xy-TPEP) at all four time points. Its tumor/liver ratio at 120 min p.i. was also significantly (p < 0.05) lower. The lipophilicity of ^{64}Cu(DOTA-Bn-xy-TPEP)$^{-}$ (log p = -1.92 ± 0.03) is close to that of ^{64}Cu(DO3A-xy-TPEP). Even though they share a similar tumor uptake, the uptake of ^{64}Cu(DOTA-Bn-xy-TPEP)$^{-}$ in the heart, liver and muscle was significantly higher at >30 min p.i. As a result, the T/B ratios of ^{64}Cu(DOTA-Bn-xy-TPEP)$^{-}$ was lower than that those of ^{64}Cu(DO3A-xy-TPEP). ^{64}Cu(NOTA-Bn-xy-TPEP) has the same overall charge as ^{64}Cu(DO3A-xy-TPEP); but its tumor uptake and tumor/heart ratios were much lower than those of ^{64}Cu(DO3A-xy-TPEP). Apparently, the BFCs and their ^{64}Cu chelates have a significant impact on both tumor uptake and T/B ratios of the radiotracer.

Linker Effects

Figure 4 illustrates a comparison of the tumor uptake and tumor/heart ratios between ^{64}Cu(DO3A-xy-TPEP), ^{64}Cu(DO3A-PEG$_2$-TPEP) and ^{64}Cu(DOTA-xy-TPEP). The addition of an extra acetamide group between DO3A and TPEP resulted in a significant reduction of liver uptake. However, the tumor/liver ratios (Table 4) of ^{64}Cu(DOTA-xy-TPEP) and ^{64}Cu(DO3A-xy-TPEP) were comparable within the experimental error, probably due to the faster tumor washout of ^{64}Cu(DOTA-xy-TPEP). Substitution of xylene with PEG$_2$ also leads to a significant reduction of the uptake in tumor and liver. As a result, ^{64}Cu(DO3A-PEG$_2$-TPEP) and ^{64}Cu(DO3A-xy-TPEP) shared very similar tumor/liver ratios.

Pet Imaging

We performed a microPET imaging study on ^{64}Cu(DO3A-xy-TPEP) using the athymic nude mice bearing U87MG glioma xenografts. Figure 5 shows microPET images of the tumor-bearing mouse administered with ~250 μCi of ^{64}Cu(DO3A-xy-TPEP) at 1, 4 and 24 h p.i. The tumor was clearly visualized as early as 1 h p.i. with very high T/B contrast. No significant radioactivity accumulation was detected in the brain, heart and muscle. After normalization, the tumor uptake of ^{64}Cu(DO3A-xy-TPEP) was 2.57 ± 0.41 %ID/g, 3.51 ± 1.20 %ID/g, and 3.11 ± 1.44 %ID/g at 1, 4 and 24 h p.i., respectively. These data are completely consistent with that observed in the *ex-vivo* biodistribution study (Figure 3), and have clearly demonstrated that ^{64}Cu(DO3A-xy-TPEP) is useful for imaging the MDR-negative tumors.

Metabolic Properties

Metabolism studies were performed on ^{64}Cu(DO3A-xy-TPEP), ^{64}Cu(DOTA-xy-TPEP), ^{64}Cu(DOTA-Bn-xy-TPEP)$^{-}$ and ^{64}Cu(NOTA-Bn-xy-TPEP) using normal mice. These four ^{64}Cu radiotracers were selected because of their difference in ^{64}Cu chelate. Since they were excreted from the renal and hepatobiliary routes, we tried to collect both urine and feces samples from the normal mice administered with the ^{64}Cu radiotracer. A reversed-phase HPLC method (Method 2) was used to analyze the collected urine and feces samples. Figure 6 shows representative radio-HPLC chromatograms of ^{64}Cu(DO3A-xy-TPEP) (left) and ^{64}Cu(DOTA-xy-TPEP) (right) in saline before injection, in urine at 30 and 120 min p.i., and in feces at 120 min p.i. There was very little metabolite (<2%) detectable for ^{64}Cu(DO3A-xy-TPEP) in both urine and feces samples. Similar metabolic stability was also observed for ^{64}Cu(DOTA-Bn-xy-TPEP)$^{-}$ and ^{64}Cu(NOTA-Bn-xy-TPEP) (Figure SII). ^{64}Cu(DOTA-xy-TPEP) is excreted without significant metabolism via renal route (Figure 6). However, only 15% of it remained intact in feces, and 85% of radioactivity appeared at 4 min. Thus, the extra acetamido group has a significant impact on metabolic stability of ^{64}Cu(DOTA-xy-TPEP) during its hepatobiliary excretion while it had no effect on its metabolic stability during renal excretion.

Transchelation of $_{64}$Cu(DO3A-xy-TPEP) in Liver

We examined the in vivo stability of ^{64}Cu(DO3A-xy-TPEP) in the liver. About 50% of total liver activity was recovered in the liver homogenate. The liver homogenate samples were analyzed using the reversed-phase and size-exclusion radio-HPLC methods. Figure SIII shows radio-HPLC chromatograms of the supernatant from liver homogenate. Using the size-exclusion HPLC method, we were able to identify four major radiometric peaks in its HPLC chromatogram (Figure SIII: bottom). While the identity of these radiometric peaks are not known, one thing is sure that ^{64}Cu(DO3A-xy-TPEP) underwent extensive tranchelation in the liver during the 2 h study period.

DISCUSSION

For the new radiotracer to be successful as a tumor imaging agent by PET or SPECT (single photon emission computed tomography), it must show a high tumor uptake. Since most of high-incidence tumors occur in torso (namely lung, colorectal and breast cancers metastatic to the lymphatic system), it is highly desirable for the radiotracer to clear from the liver and lungs so that the high T/B ratios can be achieved and clinically useful tumor images can be obtained in a short period of time. Cationic radiotracers, such as ^{99m}Tc-Sestamibi and ^{99m}Tc-Tetrofosmin, have been clinically used for imaging tumors of different origin and the transport function of MDR Pgp by SPECT (25-33). However, their cancer diagnostic values are often limited due to their insufficient tumor localization and high uptake in the non-cancerous organs, such as heart, liver and muscle, which makes it difficult to detect small lesions in the chest and abdominal regions. Radiolabeled lipophilic organic cations, such as 4-(^{18}F-benzyl) triphenylphosphonium (^{18}F-BzTPP), have also been proposed as radiotracers for tumor

imaging by PET (34-38). Their high uptake in the heart and liver may also impose a significant challenge for early detection of small tumors in the chest and abdominal regions. Thus, there is an unmet need for the radiotracers that have high tumor-selectivity (high tumor uptake with little accumulation in non-cancerous organs) and are sensitive to the mitochondrial potential changes at the early stage of tumor growth.

In our previous studies, we have demonstrated that the ^{64}Cu-labeled TPP cations, such as ^{64}Cu(DO3A-xy-TPP), are able to localize in the mitochondria of U87MG glioma cells. MicroPET imaging data also show that the tumor could be visualized clearly as early as 30 min p.i. (14). Considering both the tumor uptake selectivity, ^{64}Cu(DO3A-xy-TPP) has a significant advantage over ^{99m}Tc-Sestamibi, the radiopharmaceutical currently available for both myocardial perfusion and tumor imaging (24-33,39-45). However, the high liver uptake of ^{64}Cu(DO3A-xy-TPP) remains a significant challenge for its clinical applications as a new PET radiotracer for imaging tumors.

In this study, we used TPEP as the mitochondrion-targeting molecule. We are interested TPEP cation because of the phosphoryl group that may improve radiotracer excretion kinetics from the liver. As expected, the liver uptake of ^{64}Cu(DO3A-xy-TPEP) was significantly lower ($p < 0.01$) than that of ^{64}Cu(DO3A-xy-TPP) (Figure 3), even though ^{64}Cu(DO3A-xy-TPEP) (log P = -1.69 ± 0.11) is 10x more lipophilic than ^{64}Cu(DO3A-xy-TPP) (log P = -2.67 ± 0.21). The tumor uptake of ^{64}Cu(DO3A-xy-TPEP) is comparable to that of ^{64}Cu(DO3A-xy-TPP) at >30 min p.i. (Figure 2). As a result, tumor/liver ratios of ^{64}Cu(DO3A-xy-TPEP) are >3x better than those of ^{64}Cu(DO3A-xy-TPP). On the basis of these results, we believe that ^{64}Cu(DO3A-xy-TPEP) is a better PET radiotracer than ^{64}Cu(DO3A-xy-TPP) for imaging the MDR-negative tumors. ^{64}Cu(DO3A-xy-TPEP) also has significant advantages over ^{99m}Tc-Sestamibi with respect to the tumor uptake and T/B (tumor/heart, tumor/liver, tumor/lung and tumor/muscle) ratios.

The exact localization mechanism remains unknown even though the results from in vitro assays show that ^{64}Cu(DO3A-xy-TPP) is able to localize in mitochondria of glioma cells (14). Many factors can influence biological properties of the ^{64}Cu-labeled TPEP cations. Previously, we found that replacing DO3A in ^{64}Cu(DO3A-xy-TPP) with DO2A leads to formation of ^{64}Cu(DO2A-xy-TPP)$^{+}$, and results in a dramatic reduction in liver uptake without altering its tumor uptake. In this study, a similar reduction in liver uptake was seen for ^{64}Cu(DO2A-xy-TPEP)$^{+}$ (Figure 3); but ^{64}Cu(DO2A-xy-TPEP)$^{+}$ had a rapid tumor washout over the 2 h study period. As a result, its tumor/liver ratio is significantly lower ($p < 0.01$) than that of ^{64}Cu(DO3A-xy-TPEP).

^{64}Cu(NOTA-Bn-xy-TPEP) has the same molecular charge as ^{64}Cu(DO3A-xy-TPEP). They also share the almost identical lipophilicity with log P values being -1.69 ± 0.11 and -1.75 ± 0.03, respectively. However, the tumor uptake and T/B ratios of ^{64}Cu(NOTA-Bn-xy-TPEP) are significantly lower ($p < 0.01$) than those of ^{64}Cu(DO3A-xy-TPEP) (Figure 3). Similar adverse effect was also seen for the ^{64}Cu-labeled TPP analogs (16). Among six ^{64}Cu radiotracers evaluated in this study, ^{64}Cu(NOTA-Bn-xy-TPEP) has the lowest tumor uptake and poorest T/B ratios in non-cancerous organs, such as the heart, liver, lungs and muscle. Thus, it is reasonable to believe that the coordination geometry of the ^{64}Cu-DO3A chelates might play a significant role in tumor uptake and tumor retention of the ^{64}Cu-labeled TPP and TPEP cations.

The lipophilicity (log p = -1.92 ± 0.03) of ^{64}Cu(DOTA-Bn-xy-TPEP)$^{-}$ is also close to that of ^{64}Cu(DO3A-xy-TPEP) (log p = -1.69 ± 0.11) despite of their difference in molecular charge. Their tumor uptake (Figure 3) is comparable within the experimental error. It seems that the negative charge in^{64}Cu(DOTA-Bn-xy-TPEP)$^{-}$ does not affect its capability to localize in tumor

cells. However, the uptake of ^{64}Cu(DOTA-Bn-xy-TPEP)$^{-}$ in the heart, liver and muscle was significantly higher than that of ^{64}Cu(DO3A-xy-TPEP) at >30 min p.i. As a result, its T/B ratios was significantly lower than that ^{64}Cu(DO3A-xy-TPEP).

Linkers have a significant impact on tumor uptake and tumor/heart ratios of ^{64}Cu-labeled TPEP cations. For example, the extra acetamido group in ^{64}Cu(DOTA-xy-TPEP) results in a significantly lower liver uptake than that of ^{64}Cu(DO3A-xy-TPEP). However, the tumor/liver ratios of ^{64}Cu(DOTA-xy-TPEP) and ^{64}Cu(DO3A-xy-TPEP) compare well within the experimental error (Figure 4) due to a faster tumor washout of ^{64}Cu(DOTA-xy-TPEP). Substitution of xylene with PEG_2 leads to a significant reduction of the tumor and liver uptake. As a result, the tumor/liver ratios of ^{64}Cu(DO3A-PEG_2-TPEP) and ^{64}Cu(DO3A-xy-TPEP) are also comparable.

In addition, linkers also affect the metabolic stability of ^{64}Cu radiotracers. For example, ^{64}Cu (DO3A-xy-TPEP), ^{64}Cu(DOTA-Bn-xy-TPEP)$^{-}$ and ^{64}Cu(NOTA-Bn-xy-TPEP) have no metabolism during their excretion via renal and hepatobiliary routes as evidenced by the lack of metabolite(s) in urine and feces samples. ^{64}Cu(DOTA-xy-TPEP) remains intact during excretion via the renal excretion; but only ~15% of it remains intact in the feces sample (Figure 6). Since the only difference between ^{64}Cu(DO3A-xy-TPEP) and ^{64}Cu(DOTA-xy-TPEP) is the extra acetamido group, the metabolic instability of ^{64}Cu(DOTA-xy-TPEP) is most likely caused by the cleavage of CO-NH bond during hepatobiliary excretion.

The radioactivity detected in urine and feces samples represents only the portion excreted from the renal and hepatobiliary routes. The remaining activity is still “trapped” in organ tissues. We examined the stability of ^{64}Cu(DO3A-xy-TPEP) in the liver, and found that there was no intact ^{64}Cu(DO3A-xy-TPEP) in the liver homogenate (Figure SIII: top). While the identity of these four major radiometric peaks (Figure SIII: bottom) remains unknown, the size-exclusion HPLC chromatographic pattern of ^{64}Cu(DO3A-xy-TPEP) is very similar to that of the ^{64}Cu-labeled TETA-Octreotide in the rat liver homogenate (46). Based on the results from stability studies of ^{64}Cu complexes with tetraazamacrocycles (46-50), we believe that these radiometric peaks are likely caused by transchelation of ^{64}Cu to the proteins, such as superoxide dismutase (SOD) abundant in the liver and kidneys (51).

The metabolism of the ^{64}Cu-labeled biomolecules (antibodies and peptides) and ^{64}Cu complexes of tetraazamacrocycles has been investigated extensively (46-59). These studies clearly show that kinetic inertness of the ^{64}Cu chelate is particularly important for the *in vivo* stability of ^{64}Cu radiotracers, and their instability is often caused by transchelation of ^{64}Cu from the ^{64}Cu-BFC chelate to proteins (46,51). For target-specific ^{64}Cu radiotracers, the tumor uptake is predominantly determined by receptor binding of targeting biomolecules (antibodies or peptides). The BFCs for ^{64}Cu chelation should be those which form the ^{64}Cu-BFC chelates with high kinetic inertness in order to minimize the liver radioactivity. For the ^{64}Cu-labeled TPEP cations, however, the BFC contributes greatly to the radiotracer tumor uptake and excretion kinetics from non-cancerous organs, such as liver and lungs. The optimal BFC should be those which result in the ^{64}Cu radiotracer with high tumor uptake and the best T/B, particularly tumor/heart and tumor/liver, ratios. From this point view, DO3A and DOTA are suitable BFCs for ^{64}Cu-labeling of TPEP cations. It must be noted that the radioactivity “trapped” inside the liver due to transchelation of ^{64}Cu is only a small portion of the injected radioactivity. Whenever possible, one has to consider the radioactivity excreted from renal and hepatobiliary routes (urine and feces samples), as well as the radioactivity “trapped” in various organ tissues.

CONCLUSIONS

In summary, we evaluated six new ^{64}Cu-labeled TPEP cations for their biodistribution properties and excretion kinetics using the athymic nude mice bearing U87MG human glioma xenografts. It was found that most the ^{64}Cu radiotracers described in this study have significant advantages over ^{99m}Tc-Sestamibi with respect to their tumor/heart and tumor/muscle ratios. TPEP seems to be a better mitochondrion-targeting molecule than TPP because of the lower liver uptake and better tumor/liver ratios of ^{64}Cu(DO3A-xy-TPEP) than that of ^{64}Cu(DO3A-xy-TPP). BFCs and molecular charge also have significant impact on biological properties of ^{64}Cu-labeled TPEP cations. For example, replacing DO3A with DO2A results in ^{64}Cu(DO2A-xy-TPEP)$^{+}$, which has a lower tumor uptake and T/B ratios than ^{64}Cu(DO3A-xy-TPEP). Substitution of DO3A with NOTA-Bn has a significant adverse effect on tumor uptake of the ^{64}Cu radiotracer. However, the use of DOTA-Bn to replace DO3A has minimal impact on the radiotracer tumor uptake; but the tumor/liver ratio of ^{64}Cu(DOTA-Bn-xy-TPEP)$^{-}$ is not as good as that of ^{64}Cu(DO3A-xy-TPEP), probably due to the aromatic benzene ring in DOTA-Bn. Addition of an extra acetamido group in ^{64}Cu(DOTA-xy-TPEP) results in a lower liver uptake; but the tumor/liver ratios of ^{64}Cu(DOTA-xy-TPEP) and ^{64}Cu(DO3A-xy-TPEP) are well comparable, probably due to a faster tumor washout of ^{64}Cu(DOTA-xy-TPEP). Substitution of xylene with PEG_2 also leads to a significant reduction in both tumor and liver uptake. As a result, ^{64}Cu(DO3A-PEG_2-TPEP) and ^{64}Cu(DO3A-xy-TPEP) share very similar tumor/liver ratios. On the basis of both tumor uptake and T/B ratios of the ^{64}Cu radiotracers, we believe that both DO3A and DOTA are suitable BFCs for the ^{64}Cu-labeling of TPP cations. Among the six ^{64}Cu radiotracers evaluated in this tumor-bearing animal model, ^{64}Cu(DO3A-xy-TPEP) is of particularly interest due to its higher tumor uptake and better T/B ratios (particularly tumor/heart, tumor/liver and tumor/muscle). ^{64}Cu(DO3A-xy-TPEP) will be further evaluated for its potential as a new PET radiotracer to monitor the MDR transport function in tumors of different origin.

Supplementary Material

Refer to Web version on PubMed Central for supplementary material.

ACKNOWLEDGMENT

Authors would like to thank Dr. Sulma I. Muhammed, the Director of Purdue Cancer Center Drug Discovery Shared Resource, Purdue University, for her assistance with the tumor-bearing model. This work is supported in part by research grants: R01 CA115883 A2 (S.L.) from National Cancer Institute (NCI), R21 EB003419-02 (S.L.) from National Institute of Biomedical Imaging and Bioengineering (NIBIB) and R21 HL083961-01 from National Heart, Lung, and Blood Institute (NHLBI).

ABBREVIATIONS

DO2A, 1,4,7,10-tetraazacyclododecane-1,7-diacetic acid
DO3A, 1,4,7,10-tetraazacyclododecane-4,7,10-triacetic acid
DOTA, 1,4,7,10-tetraazacyclododecane-1,4,7,10-tetraacetic acid
NOTA, 1,4,7-triaazacyclononane-1,4,7-triacetic acid
DO2A-xy-TPP, (4-((4,10-bis(carboxymethyl)-1,4,7,10-tetraazacyclododecan-1-yl)methyl) benzyl)triphenylphosphonium
DO3A-xy-TPP, triphenyl(4-((4,7,10-tris(carboxymethyl)-1,4,7,10-tetraazacyclododecan-1-yl)methyl)benzyl)phosphonium
DO2A-xy-TPEP, (4-((4,10-bis(carboxymethyl)-1,4,7,10-tetraazacyclododecan-1-yl)methyl) benzyl)(2-(diphenylphosphoryl)ethyl)diphenylphosphonium
DO3A-xy-TPEP, (2-(diphenylphosphoryl)ethyl)diphenyl(4-((4,7,10-tris (carboxymethyl)-1,4,7,10-tetraazacyclododecan-1-yl)methyl)benzyl)phosphonium

DO3A-PEG_2-TPEP, (2-(diphenylphosphoryl)ethyl)diphenyl(4-((2-(4,7,10-tris (carboxymethyl)-1,4,7,10-tetraazacyclododecan-1-yl)acetamido)methyl)benzyl) phosphonium
DOTA-Bn-xy-TPEP, (2-(Diphenylphosphoryl)ethyl)diphenyl(4-((3-(4-((1,4,7,10-tetrakis (carboxymethyl)-1,4,7,10-tetraazacyclododecan-2-yl)methyl)phenyl)thioureido)methyl) benzyl)phosphonium
NOTA-Bn-xy-TPEP, (2-(Diphenylphosphoryl)ethyl)diphenyl(4-((3-(4-((1,4,7-tris (carboxymethyl)-1,4,7-triazonan-2-yl)methyl)phenyl)thioureido)methyl)benzyl) phosphonium

REFERENCES

(1). Kroemer G, Dallaporta B, Resche-Rigon M. The mitochondrial death/life regulator in apoptosis and necrosis. Annu. Rev. Physiol 1998;60:619–642. [PubMed: 9558479]

(2). Modica-Napolitano JS, Aprille JR. Delocalized lipophilic cations selectively target the mitochondria of carcinoma cells. Advanced Drug Delivery Reviews 2001;49:63–70. [PubMed: 11377803]

(3). Duchen MR. Mitochondria in health and disease: perspectives on a new mitochondrial biology. Mol. Aspects Med 2004;25:365–451. [PubMed: 15302203]

(4). Modica-Napolitano, JS.; Singh, KK. Mitochondria as targets for detection and treatment of cancer. Expert Reviews in Molecular Medicine. 2002. http://www.ermm.cbcu.cam.ac.uk00445-3a (short code: txt001ksb

(5). Johnson LV, Walsh ML, Chen LB. Localization of mitochondria in liver cells with rhodamine 123. Proc. Natl. Acad. Sci. USA 1980;77:990–994. [PubMed: 6965798]

(6). Summerhayes IC, Lampidis TJ, Bernal SD, Nadakavukaren JJ, Nadakavukaren KK, Shepard EL, Chen LB. Unusual retention of rhodamine 123 by mitochondria in muscle and carcinoma cells. Proc. Natl. Acad. Sci. USA 1982;79:5292–5296. [PubMed: 6752944]

(7). Modica-Napolitano JS, Aprille JR. Basis for the selective cytotoxicity of rhodamine 123. Cancer Res 1987;47:4361–4365. [PubMed: 2886218]

(8). Davis S, Weiss MJ, Wong JR, Lampidis TJ, Chen LB. Mitochondrial and plasma membrane potentials cause unusual accumulation and retention of rhodamine 123 by human breast adenocarcinoma-derived MCF-7 cells. J. Biol. Chem 1985;260:3844–3850. [PubMed: 3972850]

(9). Dairkee SH, Hackett AJ. Differential retention of rhodamine 123 by breast carcinoma and normal human mammary tissue. Breast Cancer Res. Treat 1991;18:57–61. [PubMed: 1854980]

(10). Gottlieb E, Thompson CB. Targeting the mitochondria to enhance tumor suppression. Methods in Mol. Biol 2003;223:543–554. [PubMed: 12777750]

(11). Mannella CA. The relevance of mitochondrial membrane topology to mitochondrial function. Biochim. Biophys. Acta 2006;1762:140–147. [PubMed: 16054341]

(12). Ross MF, Kelso GF, Blaikie FH, James AM, Cocheme HM, Filipovska A, Da Ros TD, Hurd TR, Smith RAJ, Murphy MP. Lipophilic triphenylphosphonium cations as tools in mitochondrial bioenergetics and free radical biology. Biochem. (Moscow) 2005;70:222–230.

(13). Jakobs S. High resolution imaging of living mitochondria. Biochim. Biophys. Acta 2006;1763:561–575. [PubMed: 16750866]

(14). Wang J, Yang C, Kim YS, Sreerama SG, Cao Q, Li Z, He Z, Chen X, Liu S. ^{64}Cu-Labeled triphenylphosphonium and triphenylarsonium cations as highly tumor-selective PET imaging agents. J. Med. Chem 2007;50:5057–5069. [PubMed: 17867662]

(15). Yang C, Li YX, Liu S. Synthesis and structural characterization of complexes of a DO3A-conjugated triphenylphosphonium cation with diagnostically important metal ions. Inorg. Chem 2007;46:8988–8997. [PubMed: 17784751]

(16). Kim YS, Yang C, Wang J, Sreerama SG, Cao Q, Li Z, He Z, Chen X, Liu S. Radiolabeled triphenylphosphonium cations as highly tumor-selective imaging agents: Effects of radiometals, bifunctional chelators and molecular charge. J. Med. Chem 2008;51:2971–2984. [PubMed: 18419113]

(17). Bähr O, Rieger J, Duffner F, Meyermann R, Weller M, Wick W. P-glycoprotein and multidrug resistance-associated protein mediate specific patterns of multidrug resistance in malignant glioma cell lines, but not in primary glioma cells. Brain Pathol 2003;13:482–494. [PubMed: 14655754]

(18). Le Jeune N, Perek N, Denoyer D, Dubois F. Influence of glutathione depletion on plasma membrane cholesterol esterification and on Tc-99m-Sestamibi and Tc-99m-Tetrofosmin uptakes; a comparative study in sensitive U87MG and multidrug-resistant MRP1 human glioma cells. Cancer Biother. Radiopharm 2004;19:411–421. [PubMed: 15453956]

(19). Bähr O, Wick W, Weller M. Modulation of MDR/MRP by wild-type and mutant p53. J. Clin. Invest 2001;107:643–645. [PubMed: 11238567]

(20). Nakatsu S, Kondo S, Kondo Y, Yin D, Peterson JW, Kaakaji R, Morimura T, Kikuchi H, Takeuchi J, Barnett GH. Induction of apoptosis in multi-drug resistant (MDR) human glioblastoma cells by SN38, a metabolite of the camptothecin derivative CPT. Cancer Chemother. Pharmacol 1997;39:417–423. [PubMed: 9054955]

(21). Wieghardt K, Bossek U, Chaudhuri P, Herrmann W, Menke BC, Weiss J. 1,4,7-Triazacyclononane-N,N',N"-triacetate (TCTA), a hexadentate ligand for divalent and trivalent metal ions. Crystal structures of [Cr^{III}(TCTA)], [Fe^{III}(TCTA)], and Na[Cu^{II}(TCTA)]·2BaBr·8H_2O. Inorg. Chem 1982;21:4308–4314.

(22). Riesen A, Zehnder M, Kaden TA. Metal complexes of macrocyclic ligands. Part XXIII. Synthesis, properties, and structures of mononuclear complexes with 12- and 14-membered tetraazamacrocycle-N,N',N'',N'''-tetraacetic acids. Helv. Chim. Acta 1986;69:2067–2073.

(23). Riesen A, Zehnder M, Kaden TA. Metal complexes of macrocyclic ligands. Part XXIV. Binuclear complexes with tetraazamacrocycle-N,N',N'',N'''-tetraacetic acids. Helv. Chim. Acta 1986;69:2074–2080.

(24). Herman LW, Sharma V, Kronauge JF, Barbarics E, Herman LA, Piwnica-Worms D. Novel hexakis (areneisonitrile)technetium(I) complexes as radioligands targeted to the multidrug resistance P-glycoprotein. J. Med. Chem 1995;38:2955–2963. [PubMed: 7636856]

(25). Agrawal M, Abraham J, Balis FM, Edgerly M, Stein WD, Bates S, Fojo T, Chen CC. Increased ^{99m}Tc-Sestamibi accumulation in normal liver and drug resistant-tumors after the administration of the glycoprotein inhibitor, XR9576. Clin. Cancer Res 2003;9:650–656. [PubMed: 12576431]

(26). Luker GD, Francisco PM, Dobkin J, Piwbica-Worms D. Modulation of the multidrug resistance P-glycoprotein: Detection with technetium-99m sestamibi in vivo. J. Nucl. Med 1997;38:369–372. [PubMed: 9074520]

(27). Liu ZL, Stevenson GD, Barrett HH, Kastis GA, Bettan M, Furenlid LR, Wilson DW, Woolfenden JM. Imaging recognition of multidrug resistance in human breast tumors using ^{99m}Tc-labeled monocationic agents and a high-resolution stationary SPECT system. Nucl. Med. Biol 2004;31:53–65. [PubMed: 14741570]

(28). Liu ZL, Stevenson GD, Barrett HH, Furenlid LR, Wilson DW, Kastis GA, Bettan M, Woolfenden JM. Imaging recognition of inhibition of multidrug resistance in human breast cancer xenografts using ^{99m}Tc-labeled sestamibi and tetrofosmin. Nucl. Med. Biol 2005;32:573–583. [PubMed: 16026704]

(29). Muzzammil T, Ballinger JR, Moore MJ. ^{99m}Tc-sestamibi imaging of inhibition of the multidrug resistance transporter in a mouse xenograft model of human breast cancer. Nucl. Med. Commun 1999;20:115–122. [PubMed: 10088159]

(30). Sharma V. Radiopharmaceuticals for assessment of multidrug resistance P-glycoprotein-mediated drug transport activity. Bioconj. Chem 2004;15:1464–1474.

(31). Vaidyanathan G, Zalutsky MR. Imaging drug resistance with radiolabeled molecules. Current Pharm. Design 2004;10:2965–2979.

(32). Filippi L, Santoni R, Manni C, Danieli R, Floris R, Schillaci O. Imaging primary brain tumor by single-photon emission computed tomography (SPECT) with technetium-99m Sestamibi (MIBI) and Tetrofosmin. Current Med. Imag. Rev 2005;1:61–66.

(33). Sharma V, Piwnica-Worms D. Metal complexes for therapy and diagnosis of drug resistance. Chem. Rev 1999;99:2545–2560. [PubMed: 11749491]

(34). Madar I, Anderson JH, Szabo Z, Scheffel U, Kao PF, Ravert HT, Dannals RF. Enhanced uptake of [^{11}C]TPMP in canine brain tumor: a PET study. J. Nucl. Med 1999;40:1180–1185. [PubMed: 10405140]

(35). Madar I, Weiss L, Izbicki G. Preferential accumulation of ^{3}H-tetraphenylphosphonium in non-small cell lung carcinoma in mice: comparison with ^{99m}Tc-MIBI. J. Nucl. Med 2002;43:234–238. [PubMed: 11850490]

(36). Min JJ, Biswal S, Deroose C, Gambhir SS. Tetraphenylphosphonium as a novel molecular probe for imaging tumors. J. Nucl. Med 2004;45:636–643. [PubMed: 15073261]

(37). Steichen JD, Weiss MJ, Elmaleh DR, Martuza RL. Enhanced in vitro uptake and retention of ^{3}H-tetraphenylphosphonium by nervous system tumor cells. J. Neurosurg 1991;74:116–122. [PubMed: 1984490]

(38). Cheng Z, Winant RC, Gambhir SS. A new strategy to screen molecular imaging probe uptake in cell culture without radiolabeling using matrix-assisted laser desorption/ionization time-of-flight mass spectrometry. J. Nucl. Med 2005;46:878–886. [PubMed: 15872363]

(39). Acampa W, Di Benedetto C, Cuocolo A. An overview of radiotracers in nuclear cardiology. J. Nucl. Cardiol 2000;7:701–707. [PubMed: 11144485]

(40). Dilsizian V. The role of myocardial perfusion imaging in vascular endothelial dysfunction. J. Nucl. Cardiol 2000;7:180–184. [PubMed: 10796009]

(41). Schwaiger M, Melin J. Cardiological applications of nuclear medicine. Lancet 1999;354:661–666. [PubMed: 10466685]

(42). Beller GA, Zaret BL. Contributions of nuclear cardiology to diagnosis and prognosis of patients with coronary artery disease. Circulation 2000;101:1468–1478.

(43). Parker JA. Cardiac nuclear medicine in monitoring patients with coronary heart disease. Semin. Nucl. Med 2001;31:223–237. [PubMed: 11430529]

(44). Saha GB, Go RT, Macintyre WJ. Radiopharmaceuticals for cardiovascular imaging. Nucl. Med. Biol 1992;19:1–20.

(45). Jain D. Technetium-99m labeled myocardial perfusion imaging agents. Semin. Nucl. Med 1999;29:221–236. [PubMed: 10433338]

(46). Bass LA, Wang M, Welch MJ, Anderson CJ. In vivo transchelation of copper-64 from TETA-Octreotide to superoxide dismutase in rat liver. Bioconj. Chem 2001;11:527–532.

(47). Boswell CA, Sun X, Niu W, Weisman GR, Wong EH, Rheingold AL, Anderson CJ. Comparative in vivo stability of copper-64-labeled cross-bridged and conventional tetraazamacrocyclic complexes. J. Med. Chem 2004;47:1465–1474. [PubMed: 14998334]

(48). Boswell CA, McQuade P, Weisman GR, Wong EH, Anderson CJ. Optimization of labeling and metabolite analysis of copper-64-labeled azamacrocyclic chelators by radio-LC-MS. Nucl. Med. Biol 2005;32:29–38. [PubMed: 15691659]

(49). Anderson CJ. Metabolism of radiometal labeled proteins and peptides: what are the real radiopharmaceuticals in vivo? Cancer Biotherapy and Radiopharm 2001;16:451–455.

(50). Sprague JE, Peng Y, Fiamengo AL, Wooden KS, Southwick EA, Wiseman GR, Wong EH, Golden JA, Rhengold AL, Anderson CJ. Synthesis, characterization and in vivo studies of Cu(II)-64-labeled cross-bridges tetraazamacrocycleamide complexes as models of peptide conjugate imaging agents. J. Med. Chem 2007;50:311–318.

(51). Bartnikas TB, Gitlin JD. Mechanisms of biosynthesis of mammalian copper/zinc superoxide dismutase. J. Biol. Chem 2003;278:33602–33608. [PubMed: 12815046]

(52). Deshpande SV, DeNardo SJ, Meares CF, McCall MJ, Adams JP, Moi MK, DeNardo GL. Copper-67-labeled monoclonal antibody Lym-1, a potential radiopharmaceutical for cancer therapy: Labeling and biodistribution in RAJI tumored mice. J. Nucl. Med 1988;29:217–225. [PubMed: 3258025]

(53). Li WP, Lewis JS, Kim J, Bugaj JE, Johnson MA, Erion JL, Anderson CJ. DOTA-D-Tyr^{1}-Octreotate: a somatostatin analogue for labeling with metal and halogen radionuclides for cancer imaging and therapy. Bioconj. Chem 2002;13:721–728.

(54). McQuade P, Miao Y, Yoo J, Quinn TP, Welch MJ, Lewis JS. Imaging of melanoma using ^{64}Cu- and ^{86}Y-DOTA-ReCCMSH(Arg^{11}), a cyclized peptide analogue of α-MSH. J. Med. Chem 2005;48:2985–2992. [PubMed: 15828837]

(55). Biddlecombe GB, Rogers BE, de Visser M, Parry JJ, de Jong M, Erion JL, Lewis JS. Molecular imaging of gastrin-releasing peptide receptor-positive tumors in mice using ^{64}Cu- and ^{86}Y-DOTA-(Pro^{1}, Tyr^{4})-Bombesin(1-14). Bioconj. Chem 2007;18:724–730.

(56). Parry JJ, Andrews R, Rogers BE. MicroPET imaging of breast cancer using radiolabeled bombesin analogs targeting the gastrin-releasing peptide receptor. Breast *Cancer Res. Treat*. 2007;101:175–183. [PubMed: 16838112]

(57). Parry JJ, Kelly TS, Andrews R, Rogers BE. In vitro and in vivo evaluation of ^{64}Cu-labeled DOTA-Linker-Bombesin(7-14) analogues containing different amino acid linker moiety. Bioconj. Chem 2007;18:1110–1117.

(58). Chen X, Liu S, Hou Y, M. Tohme M, Park R, Bading JR, Conti PS. MicroPET imaging of breast cancer α_v-integrin expression with ^{64}Cu-labeled dimeric RGD peptides. Mol. Imag. Biol 2005;6:350–359.

(59). Wu Y, Zhang X, Xiong Z, Cheng Z, Fisher DR, Liu S, Gambhir SS, Chen X. MicroPET imaging of glioma $\alpha_v\beta_3$ integrin expression using ^{64}Cu-labeled tetrameric RGD peptide. J. Nucl. Med 2005;46:1707–1718. [PubMed: 16204722]

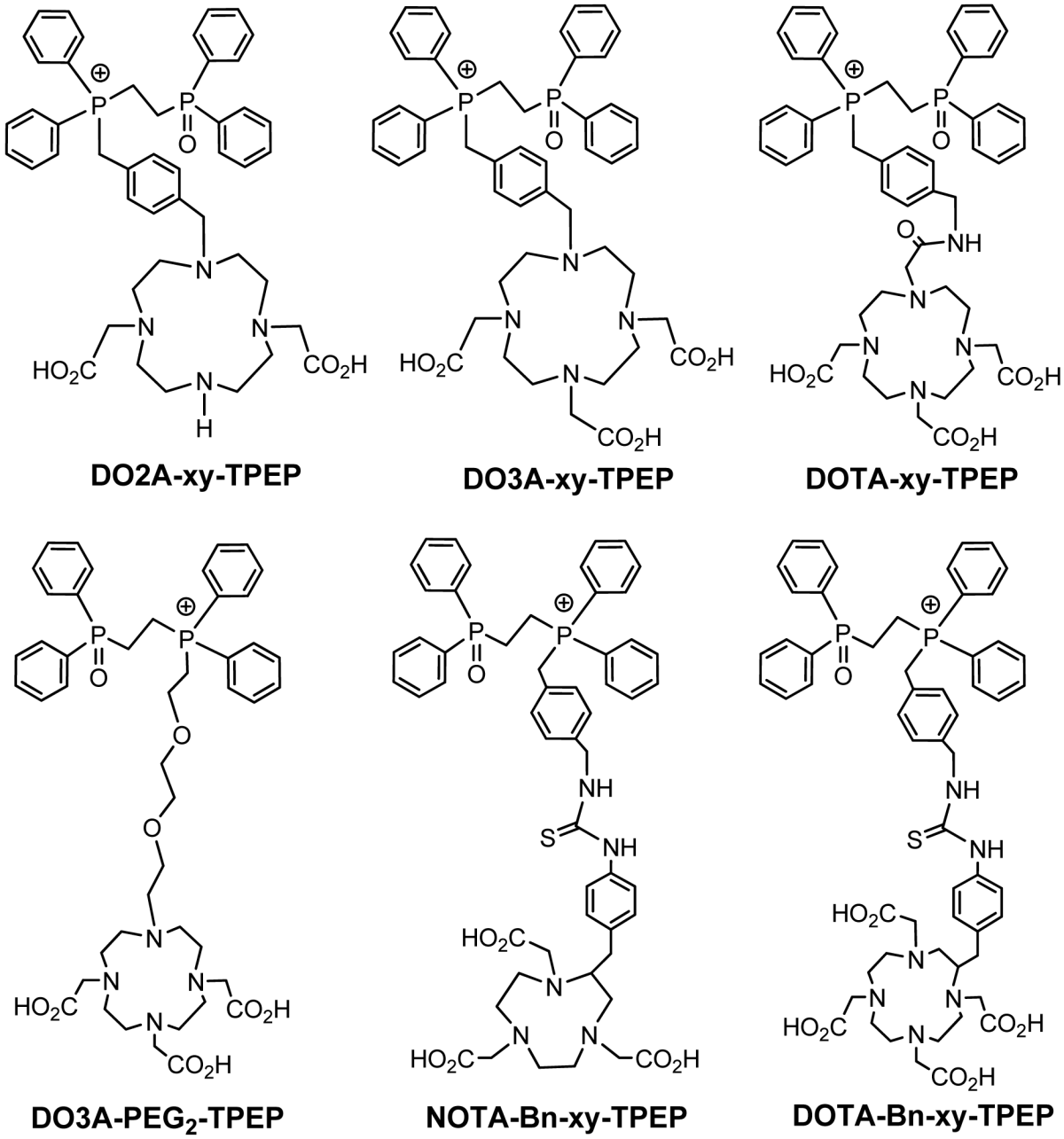

Figure 1.

TPEP conjugates for preparation of the ^{64}Cu TPEP cations useful as radiotracers for imaging tumors by PET. The TPEP moiety is used as the "mitochondrion-targeting biomolecule" to carry ^{64}Cu into tumor cells that have higher mitochondrial potential than normal cells. DO3A, DO2A, DOTA and NOTA are used as BFCs for ^{64}Cu chelation. Different linkers are used to modify pharmacokinetics and improve T/B ratios of ^{64}Cu radiotracers.

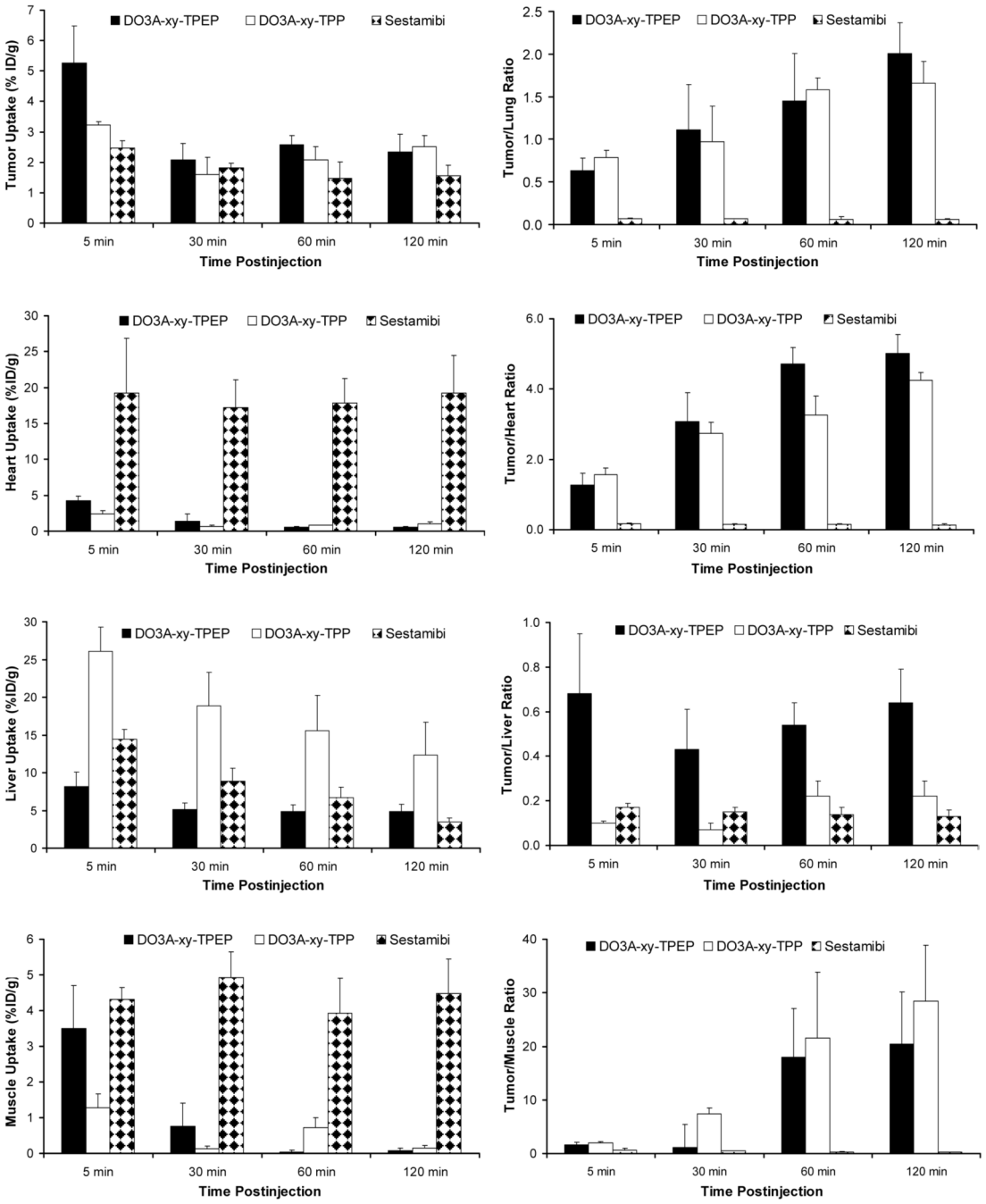

Figure 2.

Direct comparison of organ uptake and T/B ratios between ^{64}Cu(DO3A-xy-TPEP), ^{64}Cu (DO3A-xy-TPP) and ^{99m}Tc-Sestamibi in the athymic nude mice bearing U87MG human glioma xenografts.

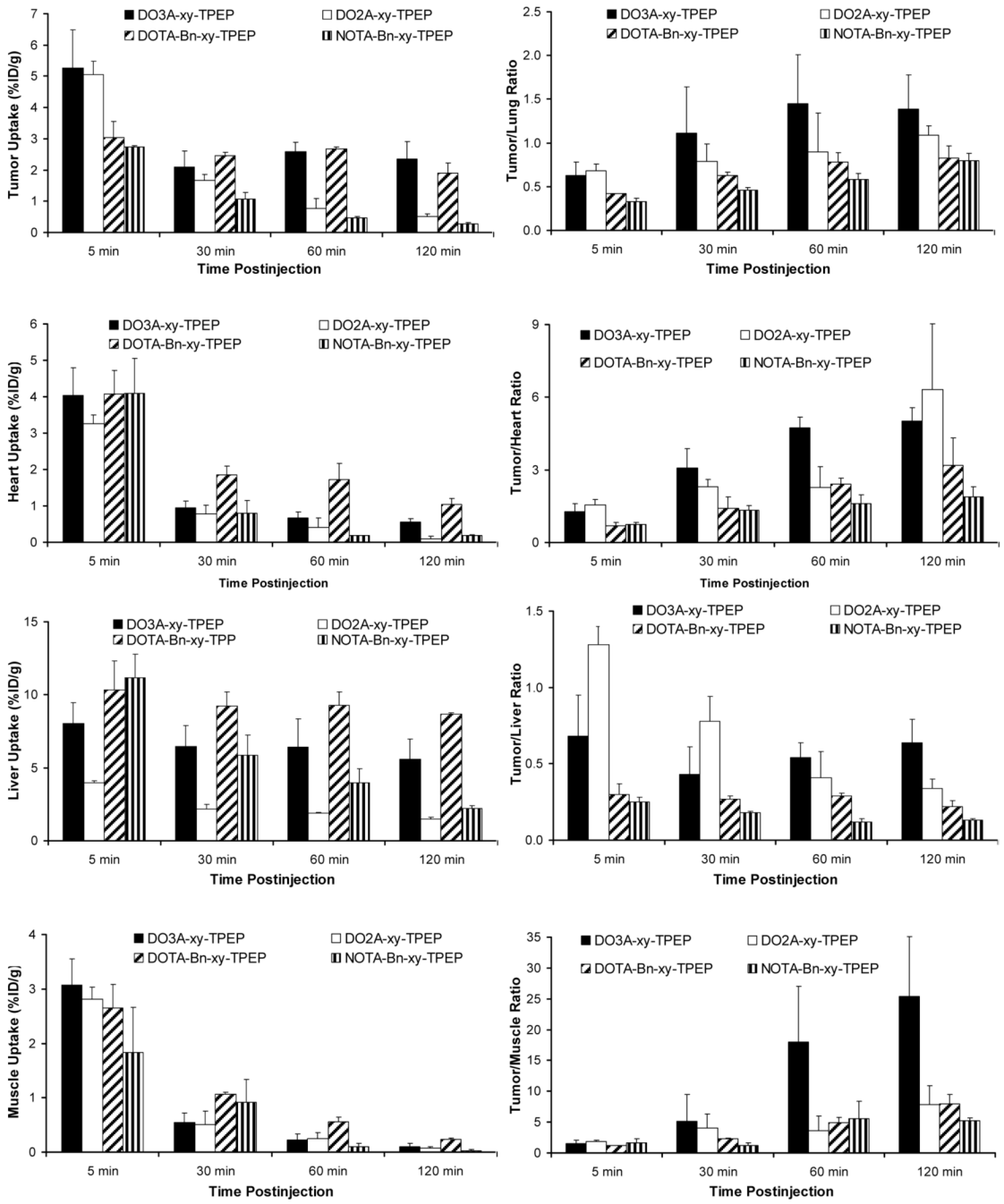

Figure 3.
Impact of BFCs on organ uptake and T/B ratios of the ^{64}Cu-labeled TPEP cations.

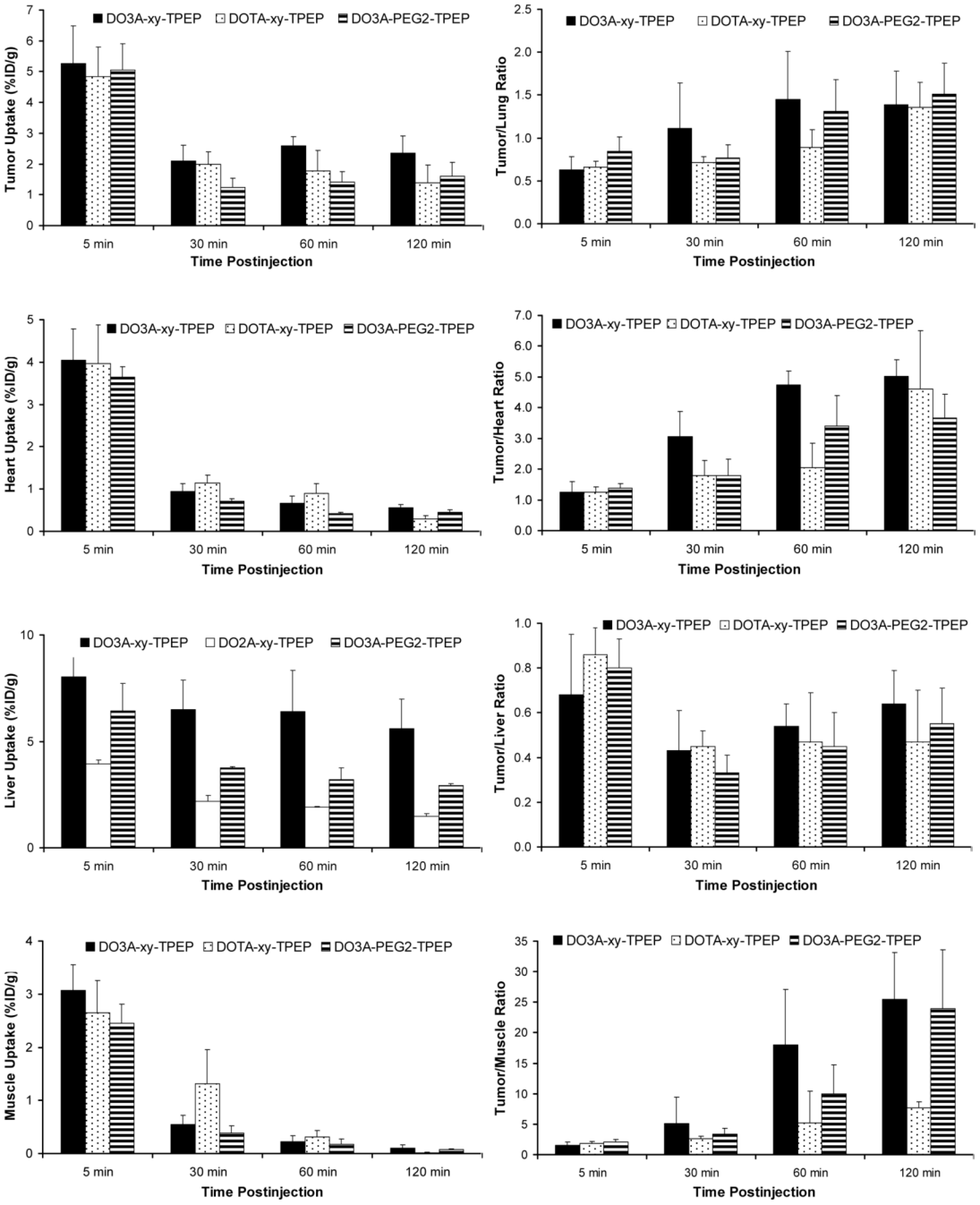

Figure 4.
Impact of the linker on organ uptake and T/B ratios of the ^{64}Cu-labeled TPEP cations.

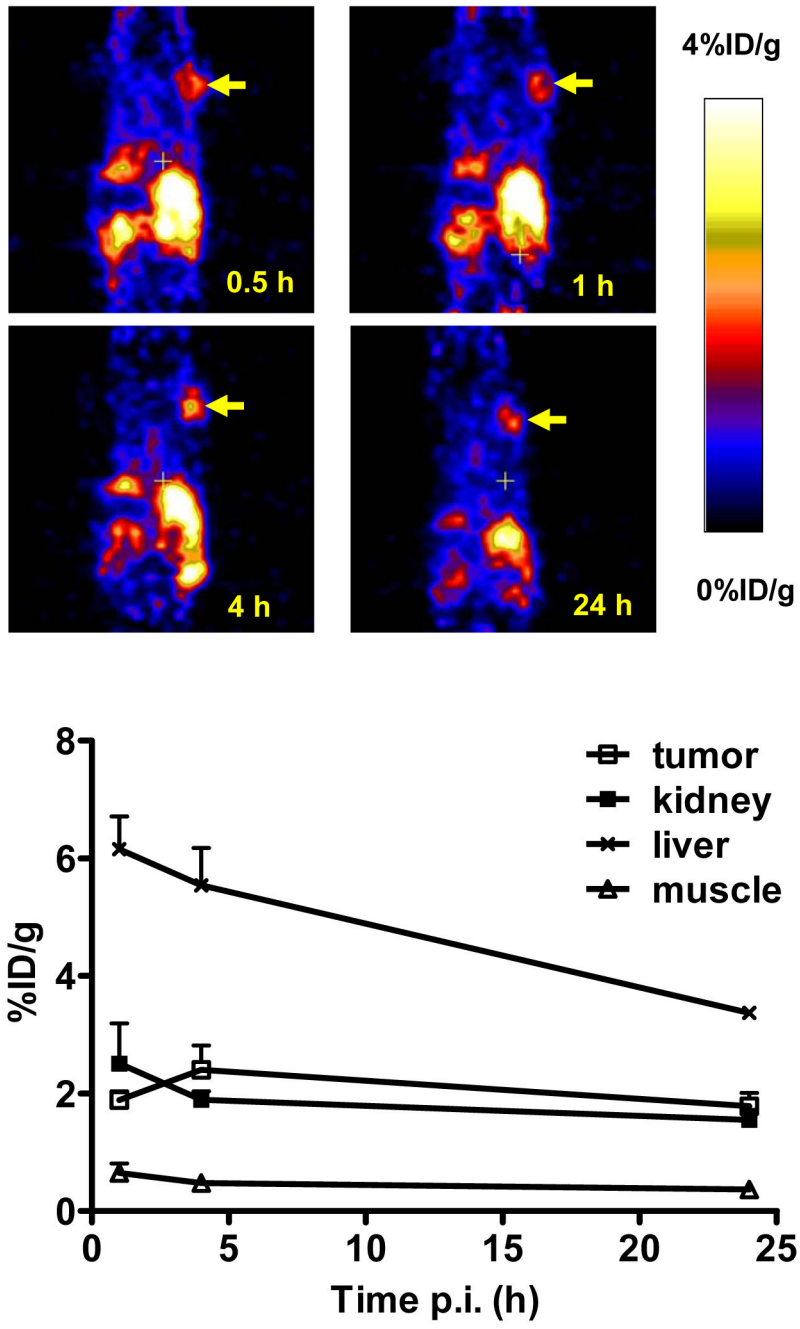

Figure 5.

The decay-corrected whole-body coronal microPET images (top) and the radioactivity accumulation quantification (n = 3, mean ± SD) in selected organs (bottom) of athymic nude mice bearing U87MG tumor administered with ~250 μCi of ^{64}Cu(DO3A-xy-TPEP). Arrows indicate the presence of glioma tumors.

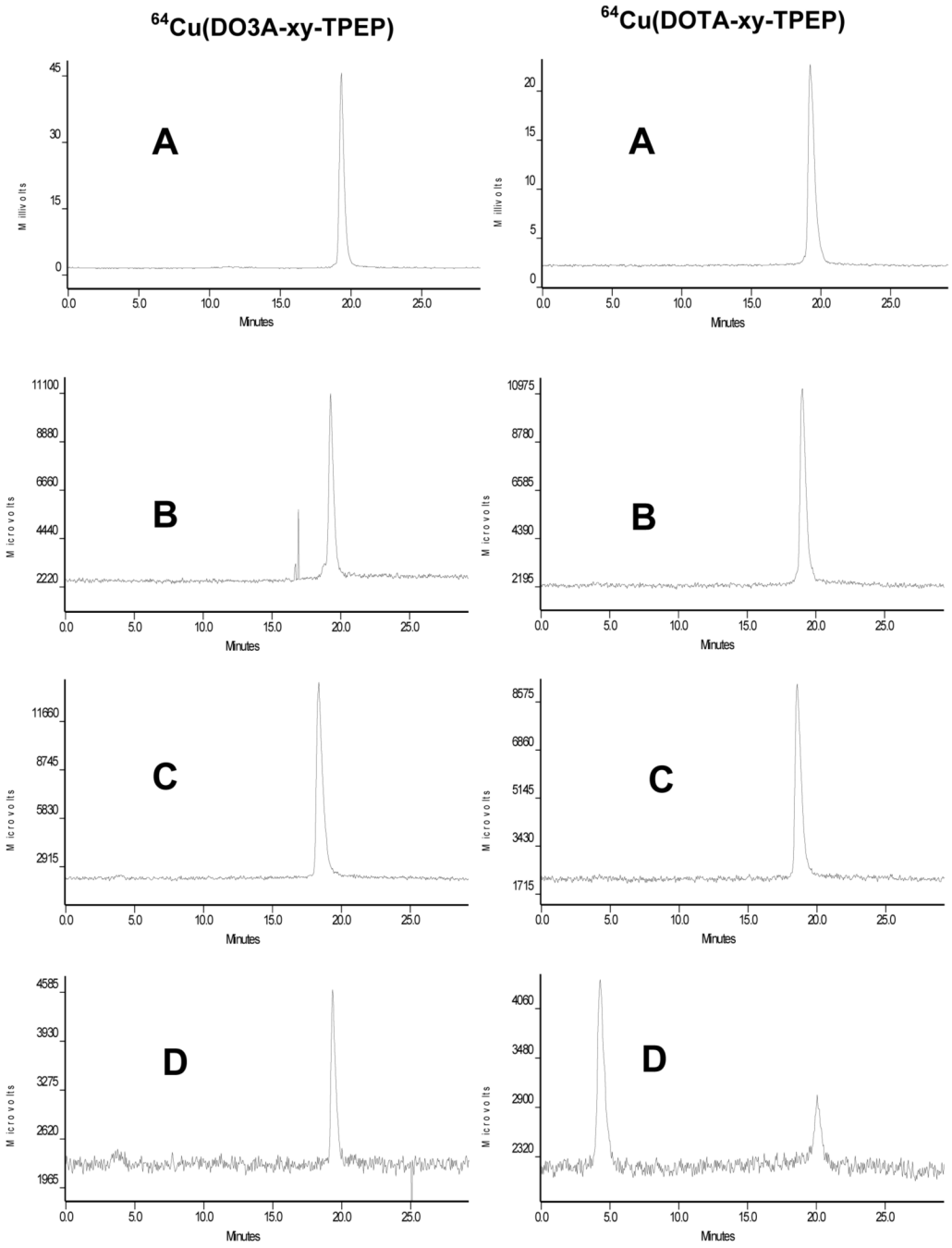

Figure 6.

Typical reversed-phase radio-HPLC chromatograms (Method 3) of ^{64}Cu(DO3A-xy-TPEP) (left) and ^{64}Cu(DOTA-xy-TPEP) (right) in saline before injection (**A**), in the urine sample at 30 min p.i. (**B**), in the urine sample at 120 min p.i. (**C**), and in the feces sample (**D**) at 120 min p.i.

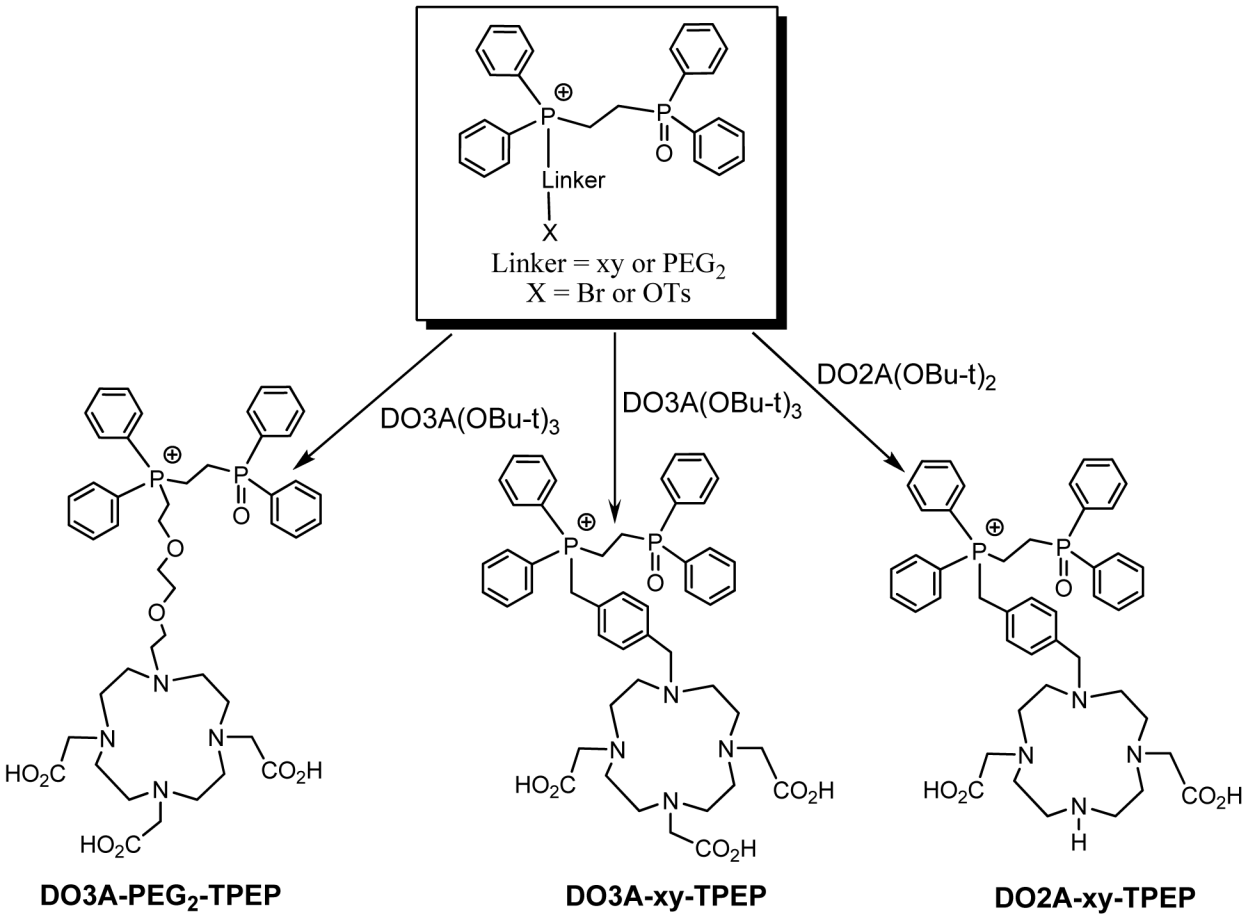

Chart I.
Synthesis of TPEP and TPPP Conjugates.

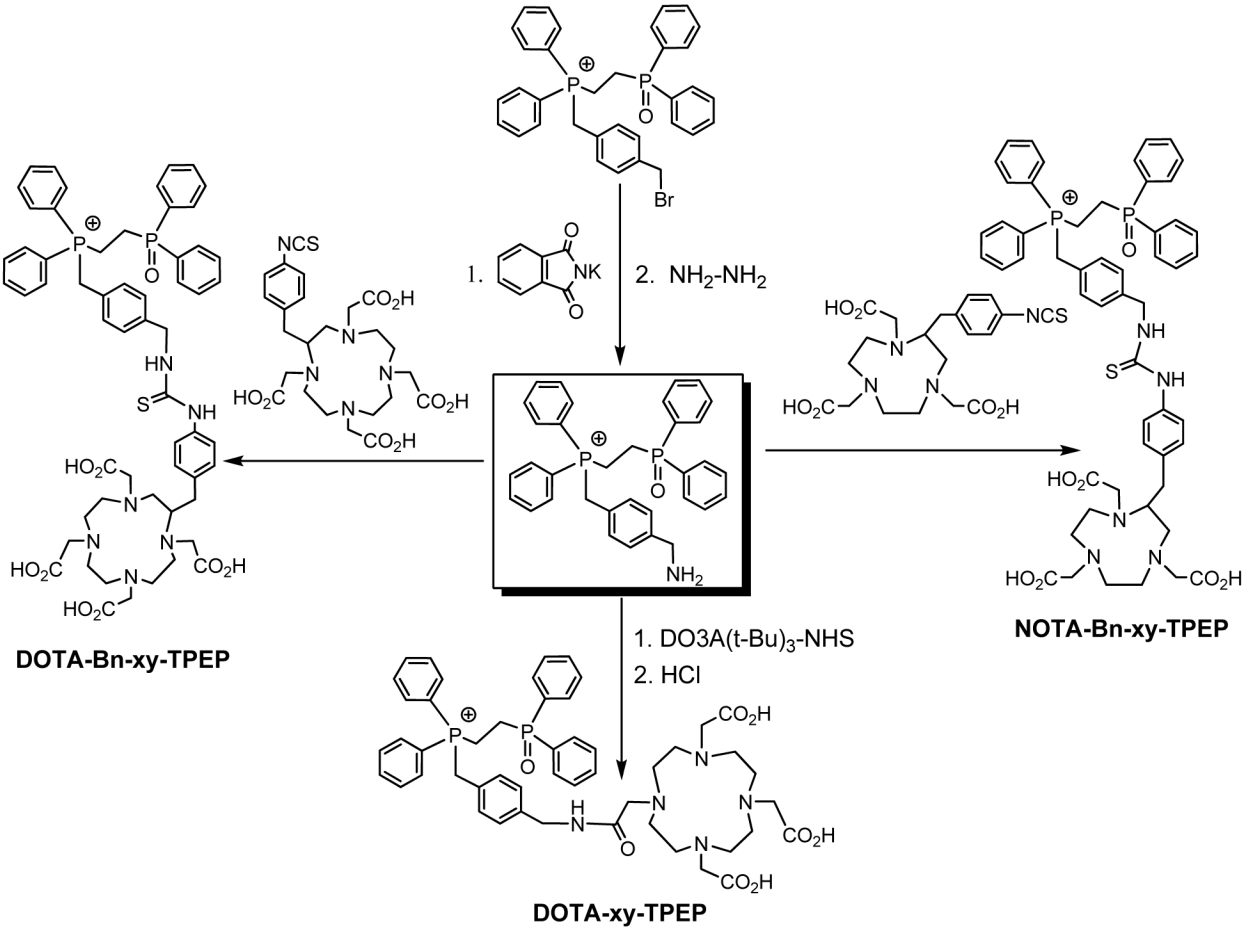

Chart II.
Synthesis of TPEP Conjugates.

Table 1

HPLC retention time and log P values for ^{64}Cu-labeled TPEP cations

Compound	RCP (%)	Retention Time (min)	Log P value
^{64}Cu(DO3A-xy-TPEP)	> 95	17.5	- 1.69 ± 0.11
^{64}Cu(DO3A-PEG$_2$-TPEP)	> 95	17.7	- 3.01 ± 0.09
^{64}Cu(DO2A-xy-TPEP)$^+$	> 95	17.5	- 1.90 ± 0.10
^{64}Cu(DOTA-xy-TPEP)	> 90	19.9	- 2.45 ± 0.02
^{64}Cu(DOTA-Bn-xy-TPEP)	> 98	20.2	- 1.92 ± 0.03
^{64}Cu(NOTA-Bn-xy-TPEP)	> 98	20.2	- 1.75 ± 0.03

Table 2

Solution stability data for the HPLC purified ^{64}Cu-labeled TPEP cations in the presence of excess EDTA (1 mg/mL in 25 mM phosphate buffer, pH = 7.5)

Time Post-Purification	0.5 h	1 h	2 h	4 h	12 h
^{64}Cu(DO3A-xy-TPEP)	99	99	98	98	97
^{64}Cu(DO2A-xy-TPEP)$^{+}$	99	98	98	97	95
^{64}Cu(DOTA-Bn-xy-TPEP)$^{-}$	99	98	99	98	97
^{64}Cu(NOTA-Bn-xy-TPEP)	99	98	99	98	97

Bioconjug Chem. Author manuscript; available in PMC 2009 October 1.

Table 3

Selected biodistribution data for ^{64}Cu radiotracers in athymic nude mice (n = 3 unless specified) bearing U87MG glioma xenografts. The organ uptake is expressed as %ID/gram

Time	Tumor	Blood	Lungs	Liver	Kidneys	Heart	Muscle
			^{64}Cu(DO3A-xy-TPEP)				
5 min	5.27±1.21	9.52±1.27	7.72±0.78	8.03±1.41	31.79±8.51	4.04±0.75	3.07±0.48
30 min	2.09±0.53	1.68±0.39	2.27±0.48	6.48±1.39	6.79±0.97	0.94±0.19	0.55±0.17
60 min	2.58±0.31	0.65±0.12	1.84±0.38	6.40±1.94	4.24±1.08	0.67±0.17	0.22±0.11
120 min*	2.35±0.57	0.36±0.07	1.51±0.18	5.59±1.39	2.98±0.53	0.55±0.09	0.10±0.06
			^{64}Cu(DO3A-PEG$_2$-TPEP)				
5 min	5.06±0.84	7.19±1.40	6.08±0.57	6.44±1.29	29.11±2.57	3.64±0.25	2.45±0.36
30 min	1.24±0.31	1.03±0.09	1.63±0.27	3.76±0.06	4.69±0.19	0.71±0.06	0.39±0.13
60 min	1.41±0.35	0.49±0.11	1.08±0.07	3.20±0.56	2.70±0.19	0.42±0.03	0.17±0.10
120 min	1.60±0.45	0.33±0.05	1.06±0.08	2.91±0.12	2.53±0.44	0.44±0.07	0.07±0.02
			^{64}Cu(DO2A-xy-TPEP)$^+$				
5 min	5.06±0.43	9.25±0.84	7.51±0.78	3.95±0.16	25.60±1.21	3.26±0.24	2.81±0.22
30 min	1.66±0.21	2.13±0.73	2.18±0.43	2.18±0.29	5.99±1.85	0.78±0.23	0.51±0.25
60 min	0.78±0.32	0.44±0.17	0.89±0.12	1.91±0.02	2.44±0.43	0.41±0.26	0.25±0.11
120 min	0.51±0.08	0.24±0.13	0.47±0.06	1.49±0.12	1.28±0.10	0.10±0.06	0.07±0.03
			^{64}Cu(DOTA-xy-TPEP)				
5 min	4.84±0.96	11.65±1.62	7.27±0.63	5.61±0.37	21.61±5.63	3.96±0.91	2.65±0.61
30 min	1.99±0.41	2.99±0.03	2.78±0.32	4.47±0.45	7.72±0.76	1.14±0.19	1.31±0.65
60 min	1.78±0.65	1.74±0.51	2.00±0.36	3.93±0.84	5.53±0.56	0.90±0.23	0.31±0.12
120 min	1.39±0.59	0.33±0.01	1.00±0.28	2.99±0.21	2.84±0.50	0.30±0.07	0.01±0.01
			^{64}Cu(DOTA-Bn-xy-TPEP)				
5 min	3.03±0.52	14.35±2.38	7.25±1.28	10.32±2.02	18.07±5.96	4.07±0.66	2.65±0.43
30 min	2.47±0.09	4.45±0.27	3.95±0.14	9.24±0.98	9.02±0.13	1.86±0.23	1.06±0.04
60 min	2.68±0.07	2.29±0.58	3.48±0.54	9.28±0.91	7.72±0.25	1.73±0.43	0.56±0.09
120 min	1.91±0.30	1.14±0.18	2.31±0.16	8.66±0.12	5.44±0.40	1.03±0.17	0.23±0.03
			^{64}Cu(NOTA-Bn-xy-TPEP)				
5 min	2.74±0.05	11.55±1.93	8.39±1.05	11.17±1.63	13.52±2.14	4.09±0.96	1.83±0.83
30 min	1.06±0.23	2.58±0.84	2.30±0.61	5.86±1.37	3.28±0.68	0.80±0.35	0.92±0.42
60 min	0.47±0.04	0.92±0.04	0.81±0.09	3.99±0.93	1.37±0.09	0.19±0.00	0.10±0.06

Time	Tumor	Blood	Lungs	Liver	Kidneys	Heart	Muscle
120 min	0.28±0.04	0.30±0.07	0.35±0.08	2.20±0.18	1.08±0.06	0.04±0.02	0.02±0.03

* n = 6 due to difficulty to determine the radiotracer uptake in muscle.

Table 4

T/B ratios for ^{64}Cu radiotracers in athymic nude mice (n = 3 unless specified) bearing U87MG human glioma xenografts

Time	Tumor/Blood	Tumor/Heart	Tumor/Lung	Tumor/Muscle	Tumor/Liver
			^{64}Cu(DO3A-xy-TPEP)		
5 min	0.57±0.13	1.26±0.34	0.63±0.15	1.57±0.49	0.68±0.27
30 min	1.48±0.52	3.06±0.82	1.11±0.53	5.08±4.37	0.43±0.18
60 min	4.66±0.65	4.73±0.45	1.45±0.56	17.96±9.11	0.54±0.10
120 min*	5.87±1.91	5.42±0.54	1.39±0.39	20.42±9.72	0.64±0.15
			^{64}Cu(DO3A-PEG$_2$-TPEP)		
5 min	0.72±0.15	1.38±0.16	0.84±0.17	2.09±0.39	0.80±0.13
30 min	1.21±0.31	1.78±0.54	0.77±0.15	3.38±0.96	0.33±0.18
60 min	2.99±1.03	3.40±1.00	1.31±0.37	9.99±0.4.74	0.45±0.15
120 min	4.83±1.05	3.66±0.77	1.51±0.36	23.95±9.63	0.55±0.16
			^{64}Cu(DO2A-xy-TPEP)$^+$		
5 min	0.55±0.06	1.55±0.14	0.68±0.08	1.81±0.23	1.28±0.12
30 min	0.87±0.37	2.30±0.83	0.79±0.20	4.04±2.24	0.78±0.16
60 min	1.94±0.84	2.26±1.00	0.90±0.44	3.64±2.35	0.41±0.17
120 min	2.63±1.47	6.32±2.92	1.09±0.11	7.83±3.05	0.34±0.06
			^{64}Cu(DOTA-xy-TPEP)		
5 min	0.41±0.04	1.24±0.18	0.66±0.07	1.86±0.36	0.86±0.12
30 min	0.67±0.14	1.78±0.51	0.71±0.07	1.65±0.39	0.45±0.07
60 min	1.08±0.46	2.05±0.79	0.89±0.21	5.18±1.17	0.47±0.22
120 min	4.21±1.66	4.61±1.90	1.36±0.29	7.65±1.04	0.47±0.23
			^{64}Cu(DOTA-Bn-xy-TPEP)		
5 min	0.21±0.04	0.75±0.08	0.42±0.06	1.15±0.07	0.30±0.07
30 min	0.56±0.04	1.34±0.17	0.63±0.04	2.32±0.07	0.27±0.02
60 min	1.21±0.26	1.61±0.36	0.78±0.11	4.92±0.83	0.29±0.02
120 min	1.69±0.26	1.88±0.43	0.83±0.14	8.00±1.54	0.22±0.04
			^{64}Cu(NOTA-Bn-xy-TPEP)		
5 min	0.24±0.03	0.69±0.14	0.33±0.04	1.68±0.63	0.25±0.03
30 min	0.42±0.07	1.42±0.47	0.46±0.03	1.25±0.36	0.18±0.01
60 min	0.51±0.03	2.42±0.25	0.58±0.07	5.59±2.86	0.12±0.02
120 min	0.94±0.19	3.19±1.12	0.80±0.08	5.22±0.40	0.13±0.01

Bioconjug Chem. Author manuscript; available in PMC 2009 October 1.

Time	Tumor/Blood	Tumor/Heart	Tumor/Lung	Tumor/Muscle	Tumor/Liver

* n = 6 due to difficulty to determine the tumor/muscle muscle ratios.